



Ecosystem-scale biogenic volatile organic compound fluxes over rapeseed by eddy-covariance

Pauline Buysse^{1,2}, Florence Lafouge¹, Raluca Ciuraru¹, Brigitte Durand¹, Olivier Zurfluh¹, Céline Décuq¹, Olivier Fanucci¹, Lais Gonzaga Gomez¹, Jean-Christophe Gueudet¹, Sandy Bsaibes³, Nora Zannoni^{3,4}, Valérie Gros³, Benjamin Loubet¹

¹Université Paris Saclay, INRAE, AgroParisTech, UMR ECOSYS, Palaiseau, 91120, France

²now at INRAE-Institut Agro, UMR SAS, Rennes, 35000, France

³UMR CNRS-CEA-UVSQ, Université Paris Saclay, IPSL, LSCE, Gif-sur-Yvette, 91190, France

⁴now at Institute of Atmospheric Sciences and Climate, National Research Council, Bologna, 40129, Italy

10 *Correspondence to:* Pauline Buysse (pauline.buysse@inrae.fr)

Abstract. Biogenic volatile organic compounds (BVOC) are key precursors of ozone and secondary organic aerosols, yet their emissions from croplands remain poorly characterized. Here, we report what is, to our knowledge, the first ecosystem-scale quantification of BVOC fluxes over a rapeseed crop during fruit development and senescence. Measurements were conducted at the FR-Gri ICOS site near Paris (France) in May–June 2017 using eddy covariance with a proton-transfer-reaction quadripole ion guide time-of-flight mass spectrometer (PTR-Qi-TOF-MS). Complementary flux estimates were obtained via an aerodynamic resistance approach using a five-level vertical concentration profile. In total, 42 BVOC were significantly emitted or deposited. Methanol dominated emissions during fruit development (about 90 % of total molar flux), followed by acetone, monoterpenes and isoprene. During senescence, formaldehyde and methanethiol emerged as additional contributors. Deposition fluxes were mainly attributed to formic acid (about 50 %), with smaller contributions from other oxygenates. Several BVOC, including formaldehyde and acetic acid, exhibited bidirectional fluxes. Agreement between aerodynamic resistance and eddy-covariance fluxes was generally acceptable for non-reactive BVOC (R^2 ranging 5–31 %), but diverged for reactive compounds due to longer residence times in profile tubing. This effect helped reveal episodic, atypical deposition of monoterpenes, isoprene, and siloxanes, likely linked to herbicide-related advection from neighbouring fields. Our findings eventually demonstrate that BVOC contribution to total OH reactivity is mostly due to terpenoids (about 40 %), suggesting that MEGAN2.1 would substantially underestimate terpenoid emissions from oilseed rape, implying a larger role of croplands in secondary organic aerosol formation than currently represented.

1 Introduction

30 Volatile organic compounds (VOCs) only make up a small fraction of air composition and are negligible greenhouse gases, but they play an important role in atmospheric chemistry and have an indirect effect on climate (Isaksen et al., 2009; Peñuelas and Staudt, 2010). Indeed, in the presence of nitrogen oxides and solar radiation, these compounds can form ozone, a greenhouse gas and pollutant (Atkinson and Arey, 2003; Sartelet et al., 2012). They are also precursors of secondary organic aerosols (SOA) when influenced by solar radiation and meteorological parameters like temperature and humidity (Mahilang et al., 2021; Sakulyanontvittaya et al., 2008). Also, by reducing the oxidative capacity of the atmosphere through the consumption of OH radicals, they can increase methane lifetime in the troposphere (Kaplan et al., 2006; Stevenson et al., 2020; Boy et al., 2022). Furthermore, BVOC may affect health directly; such as terpenoids



that may cause allergies (Butcher et al., 1994, 1995; McEwan and Macfarlane Smith, 1998), or carbonyl compounds and methyl halides that may be harmful to the environment, respectively due the phytotoxic characteristics of the compounds they contribute to form, and to their contribution to the ozone layer destruction (Müller et al., 2002; Jiao et al., 2020).

VOC emissions can be either anthropogenic or biogenic (BVOC), the latter representing up to 90 % of the total emissions (Guenther et al., 1995) globally. According to Karl et al. (2009), in Europe forests contribute 55 % of total BVOC emissions from terrestrial ecosystems and agricultural lands to 27 %. Forests are strong emitters of the two most contributing BVOC species, isoprene and monoterpenes (Sindelarova et al., 2014), while croplands mostly release oxygenated BVOC like methanol and acetone (Bachy et al., 2016, 2018, 2020; Das et al., 2003; Gonzaga Gomez et al., 2019; Graus et al., 2013; Havermann et al., 2022; Loubet et al., 2022; Wiß et al., 2017). As forests are the largest emitters of terpenoids globally (reactive compounds that significantly impact atmospheric chemistry), forests have been more studied than agricultural ecosystems. However, better quantification of BVOC exchanged fluxes in agricultural ecosystems is needed and started a decade ago. The variety of crop species and phenological stages have to be considered and documented to improve regional and global BVOC emission estimates, as they greatly influence the type and magnitude of BVOC emissions (Courtois et al., 2009; Manco et al., 2021; Vivaldo et al., 2017). For example, the MEGAN2.1 model (Guenther et al., 2012) gathers all crop species into a unique “crop” category so that BVOC emission factors reflect neither the variety among crop species nor the phenological stages of the crops.

Among the main crop species in Europe, wheat and maize are the crop species in which BVOC emissions have been the most widely quantified from the leaf to the ecosystem scale and through laboratory experiments (Mozaffar et al., 2018; Piesik et al., 2011) and field campaigns (Bachy et al., 2016, 2020; Gallagher et al., 2000; Gomez et al., 2021; Gonzaga Gomez et al., 2019; Morrison et al., 2016). However, although rapeseed represents a large share of oilseed production in France, Europe, and the world, data on BVOC emissions from rapeseed plants and fields are scarce. France is indeed the first country in Europe in rapeseed production. Europe is the world leader (30 %) in this crop production (Woźniak et al., 2019), with rapeseed representing the most significant share of oilseed production (63 %) in Europe and the second most important one after soya bean in the world (FAOSTAT, 2023). Early BVOC studies performed on rapeseed, using adsorption on Tenax-TA tubes and gas chromatography-mass spectrometry (GC-MS) analysis, provided estimations of BVOC compounds emitted (Butcher et al., 1994, 1995) and their relative mixing ratios (Konig, 1995; McEwan and Macfarlane Smith, 1998). The former reported the emission of oxygenated BVOC, together with terpenoid-like compounds, and the latter showed that flowering rapeseed was emitting various types of terpenes, together with a few sulphur compounds. Later, Müller et al. (2002), using the cuvette technique, self-filled stainless steel adsorption tubes and subsequent GC-MS analysis, quantified emission fluxes of monoterpenes and carbonyl compounds. They also pointed out the significant difference between the fluxes measured in earlier studies and their work, likely attributed to differences in measurement techniques. Gonzaga Gomez et al. (2019) and, more recently, Havermann et al. (2022) performed direct chamber measurements on rapeseed plants in the field. The latter reported emission fluxes for 25 BVOC using a proton transfer reaction quadrupole mass spectrometer (PTR-QMS 500), and the former, using the “Time-Of-Flight” technology with a PTR-Qi-TOF-MS that allows for the compounds to be detected simultaneously at a high frequency (10 Hz), managed to detect over more than 400 significant BVOC exchanged by rapeseed plants. However, while the quantification of BVOC flux exchanges at the ecosystem or field scale, using eddy-covariance setups, has already been performed successfully in forests (Acton et al., 2016; Brillì et al., 2014a, 2016; Gallagher et al., 2000; Park et al., 2013, 2014; Jensen et al., 2018; Millet et al., 2018; Schallhart et al., 2016, 2018; Sarkar et al., 2020), grasslands (Bamberger et al., 2011; Ruuskanen et al., 2011), maize and wheat crops (Bachy et al.,



2016, 2018, 2020; Karl et al., 2001 (virtual disjunct eddy-covariance); Loubet et al., 2022), and even more recently to
80 a shallow lake at a peatland site (Seco et al., 2020) and urban areas (Acton et al., 2020), such information for rapeseed
crops is, to our knowledge, still missing. Compared to chamber measurements, eddy-covariance allows (i) to integrate
the whole ecosystem over several hectares (generally from about 4 ha up to 60-70 ha in forested areas), including the
canopy and the soil, without disturbing the ecosystem (ii) to detect more reactive species given the shorter residence
time in the inlet tube than in chambers, and (iii) to quantify deposition fluxes, which is challenging in chambers due to
85 long residence time, interactions with chamber surfaces, and is even not possible when chambers are filled with zero
air.

The objectives of this study were, with the use of an eddy-covariance setup integrating a PTR-Qi-TOF-MS, i) to identify
the main exchanged BVOC from a rapeseed field during the late vegetation development stages, ii) to quantify BVOC
fluxes (emission and deposition) at the field scale using the eddy-covariance technique, iii) to provide emission factors
90 specific to rapeseed, therefore contributing to improve modelled BVOC emissions in croplands, and iv) to evaluate the
potential effect of these emissions on OH reactivity in the atmosphere, relative to existing emission factors.

2 Material and Methods

2.1 Measurement site

The field campaign took place at the Grignon FR-Gri site (48.9°N, 1.95°E; elevation 125 m), about 40 km west of Paris
95 (France). The site is part of the European ICOS network (Integrated Carbon Observing System, www.icos-ri.eu). It
consists of a 19-ha field on a relatively flat plateau with a gentle slope of approximately 1 % towards the northeast. The
soil is classified as silt loam (10 % sand, 71% silt, 19% clay) in the cultivated layer. The site is surrounded by other
agricultural fields and a mixed farm with animal houses to the southwest (at around 400 m distance). The farm livestock
is substantial, with about 200 cows and 500 sheep and a production of 900 lambs per year on average. As shown by
100 earlier studies at the same site (Kammer et al., 2020; Loubet et al., 2011, 2022), both the animal house and the fields
are a large source of ammonia and a significant source of VOCs, among which methanol, ethanol and acetaldehyde,
together with trimethylamine and dimethylsulfide. The field is also bordered by a road with heavy traffic located at
more than 900 m to the east and other roads with less traffic to the north (300 m) and west (700 m), which were shown
to be sources of NO_x (Vuolo et al., 2017). Loubet et al. (2011) give more details about the site.

105 The field is managed with the following crop rotation: maize, winter wheat, winter barley, and mustard as a catch crop,
and with reduced tillage since 2000. Rapeseed (*Brassica napus* L.) is also sown occasionally at the field site, such as in
August 2012 and 16 August 2016 (Bohême variety) for the present field campaign. The field usually receives a variable
amount of nitrogen ranging between 150 and 300 kg N ha⁻¹ y⁻¹, mainly as nitrogen solution and cattle manure (usually
once every 3 years; the last application was on 12 August 2016). Before the present campaign, the field received 3 times
110 39 kg N ha⁻¹ of urea ammonium nitrate solution (UAN, 5% NO₃, 25% NH₄ and 50% CO(NH₂)₂, applied on 20 February,
3 March and 22 March 2017), two insecticide applications (12 and 28 March 2017, 0.05 l ha⁻¹, MAGEOS®, Alpha-
Cypermethrin 15%) and a fungicide application (15 April, 0.4 l ha⁻¹, FILAN SC®, 200 g/l Boscalid and 200 g/l
Dimoxystrobin). The preceding crop was winter wheat, harvested in July 2016. Rapeseed was harvested on 30 July
2017. The average above-ground rapeseed biomass sampled and determined at the maturity stage (19 April, 2017) was
115 781 ± 188 g m⁻².

2.2 Eddy-covariance BVOC fluxes

BVOC fluxes were measured almost continuously (a few interruptions being due to technical problems with the set-up)
from 9 May to 30 June 2017 with the eddy-covariance (EC) method, this period corresponding to mature and senescent



- rapeseed vegetation (BBCH stages from 70s to 90s, see section 2.5.2). The experimental setup was part of a larger
 120 BVOC mixing ratio measurement campaign with profile measurements (see section 2.3), and chamber measurements
 (Gonzaga Gomez et al., 2019), similar to the campaign described in Loubet et al. (2022). Air was sampled at 3 m height
 through a 50 m-60 °C-heated PFA tube at 50 NL min⁻¹ with a SV-1010 pump (Busch, Switzerland). The three
 components of the wind velocity (u, v, w) and the sonic temperature were recorded at 20 Hz with an ultrasonic
 anemometer (model R3-50, Gill Instruments Ltd., UK), 20 cm apart from the air inlet.
- 125 BVOC mixing ratios were measured at 10 Hz with a PTR-Qi-TOF-MS (Ionicon, Innsbruck, Austria), operated at the
 same conditions as in Gonzaga Gomez et al. (2019). In the drift tube, the pressure P_d was set to 4 ± 0.01 mbar, the drift
 temperature T_d to 80 ± 0.06 °C, and the drift voltage E to 995 ± 0.03 V, while the extraction voltage at the end of the
 tube U_{Dx} was 44 ± 0.20 V. These conditions ensured an E/N ratio (where N is the number density of the gas molecules
 in the drift tube) of 132 ± 0.03 Td (1 Td = 10^{-17} V cm⁻²). Once extracted from the drift tube, the protonated ions were
 130 pulsed and separated according to their mass-to-charge (m/z) ratio at a rate of 25 kHz, leading to 2500-extracted spectra
 per 100 ms. The detection channels were set to 240 000, and the mass spectrum spanned from m/z 15 to m/z 530. BVOC
 were identified based on expert knowledge. Many BVOC could not be unequivocally identified.

The raw data (in counts per second, cps) from the PTR-Qi-TOF-MS were synchronized with the ultrasonic anemometer
 data at 20 Hz by a Labview program. In practice, each integrated ion peak was updated in the Labview acquisition
 135 system as soon as produced by the PTR-Qi-TOF-MS software. Files containing 5 min of synchronized data were stored
 for post-computation. Mixing ratios for each BVOC i (C_i) were computed following the same procedure as the one
 described in Loubet et al. (2022). The uncorrected mixing ratio of the compound $C_{i,ptr}$ (ppb) was calculated using:

$$C_{i,ptr} = 1.657e^{-11} \times \frac{U_{drift} T_{drift}^2}{2} \times \frac{cps_{R_iH^+}^{trans}}{cps_{H_3O^+}^{trans} + cps_{H_2O \cdot H_3O^+}^{trans}} \quad (1)$$

$k p_{drift}$

$$cps_{R_iH^+}^{trans} = \frac{TR_{H_2O^+}}{TR_{R_iH^+}} \times cps_{R_iH^+} \quad (2)$$

- 140 where U_{drift} is the voltage of the drift tube (V), T_{drift} is the drift tube temperature in kelvin (K), p_{drift} is the pressure in the
 drift (mbar), k is the proton transfer reaction rate assumed to be constant for all compounds (2.5×10^{-9} cm³ s⁻¹), $cps_{R_iH^+}$
 is the cps of the product ion i , $cps_{H_3O^+}$ and $cps_{H_2O \cdot H_3O^+}$ are the cps of the source ion and the first water cluster, *trans*
 stands for corrected for transmission, $TR_{H_3O^+}$ is the transmission factor for H_3O^+ , $TR_{R_iH^+}$ is the transmission factor for
 the product ion i , both determined by the transmission curve (see Table S01 in supplementary material). The values of
 145 $cps_{H_3O^+}^{trans}$ was computed from ion m/z 21.022 ($H_3^{18}O^+$) by multiplying by the isotopic factor of O^{18} / O^{16} in water
 (487.56). The constant $1.657e^{-11}$ was derived from the PTR-Qi-TOF-MS setup.

The calibrated mixing ratio C_i was then computed by subtracting the zero-air mixing ratio $C_{i,ptr}^{zero\ air}$ and multiplying by
 a calibration coefficient, similarly as in Loubet et al. (2022), following:

$$C_i = S_{toluene}(t) \times \frac{S_i(t_0)}{S_{toluene}(t_0)} \times (C_{i,ptr} - C_{i,ptr}^{zero\ air}) \quad (3)$$

- 150 The calibration coefficient was computed as a product of a time-evolving calibration coefficient of toluene $S_{toluene}(t)$
 and a species-specific calibration coefficient $S_i(t_0)$ normalised to toluene computed during the one-off calibration
 before the campaign or taken from the Koss et al. (2018) dataset. $S_{toluene}(t)$ was computed as the slope of the regression
 (with intercept forced to zero) between $C_{toluene,ptr}$ and the prescribed mixing ratio of toluene during periodic
 calibrations with a cylinder containing 102 ppbv of benzene, 104 ppbv of toluene, 130 ppbv of ethylbenzene and 336



155 ppbv of xylene (122 ppbv ortho, 121 ppbv meta, 123 ppbv para; BTEX, Messer, France). Only toluene was used because
 other compounds had confounding fragments. Gas from this cylinder was diluted with synthetic air (alphagaz 1, Air
 Liquide, France) using a fluorinert coated mass flow controller (Bronkhorst, The Netherlands). The calibration factor
 $S_{toluene}(t)$ varied between 2.11 ± 0.015 on 4 May and 2.37 ± 0.029 on 23 June (see Table S01 in Supplementary
 Material for details). For a few BVOC, we made a one-off calibration with a standard cylinder containing 14 compounds
 160 (containing, 990 ppb methanol, 990 ppb acetonitrile, 950 ppb acetaldehyde, 1000 ppb ethanol, 1010 ppb acroleine, 980
 ppb acetone, 950 ppb isoprene, 1010 ppb crotonaldehyde, 990 ppb 2-butanone, 990 ppb benzene, 990 ppb toluene, 1020
 ppb o-xylene, 1010 ppb chlorobenzene, 1010 ppb α -pinene, 1020 ppb 1,2- dichlorobenzene, Ionicon, Austria) and for
 methanol by comparing against a PTR-HR-MS that returned from an ACTRIS inter-comparison exercise (Holzinger et
 al., 2019). The calibration factors are given in Table S02 in supplementary material. The calibration factors reported by
 165 Koss et al. (2018) were used to compute the calibration factors for 145 other compounds, as a compromise discussed in
 Loubet et al. (2022). Individual calibration factors from the one-off calibration and Koss et al. (2018) were reported as
 fractions relative to the toluene calibration factor to be used in equations (3) and (4) (Table S02). The background
 mixing ratio $C_{i,ptr}^{zero-air}$ was determined every 30 minutes by passing the sampled air through a hydrocarbon filter
 (Supelco ref 22445-12) for 2 minutes, averaging the last 30 seconds.

170 The BVOC eddy covariance flux was computed based on standard eddy-covariance procedures following Loubet et al.
 (2022):

$$F_i = \frac{\overline{p_a^d}}{R\overline{T_a}} \overline{w' C_i'} \quad (4)$$

Where F_i is the flux ($\text{nmol m}^{-2} \text{s}^{-1}$), w is the vertical wind component (m s^{-1}), $\overline{T_a}$ is the air temperature (K), $\overline{p_a^d}$ is the
 dry air pressure (Pa), and R is the ideal gas constant ($8.31 \text{ J mol}^{-1} \text{ K}^{-1}$). Overbars ($\overline{\quad}$) denote averages, and primes
 175 denote fluctuations around the mean following Reynolds decomposition rules. Here w' was calculated by applying two
 rotations following Aubinet et al. (2000). The covariance between C_i' and w' was calculated after dephasing the two
 signals with a lag time τ computed as the time at which the correlation function $\overline{w'(t)C_i'(t-\tau)}$ was the largest in
 absolute value (Langford et al., 2015). The time lag was 3.55 s and did not differ between a selection of BVOC and was
 therefore set equal for all of them.

180 The random uncertainty on the flux (RU_i) was calculated as the standard deviation over a 10 s period of the covariance
 function $\text{corr}_{w'c_i'}(t)$ around $t = 80\text{s}$ and $t = -80\text{s}$ as described by Spirig et al. (2005). The mean hourly fluxes ($\overline{F_i^h}$)
 and random uncertainty $\overline{RU_i^h}$ were computed based on the 5-min data. The flux was averaged, but the random
 uncertainty was computed using a quadratic mean (Langford et al., 2015) as :

$$\overline{RU_i^h} = \frac{1}{N} \sqrt{\sum_{i=1}^N RU_i^2} \quad (5)$$

185 Where N is the number of 5-min periods in an hour, which was 8 or below since 20 min per hour was dedicated to
 profile and calibration measurements.

Flux high-frequency losses generated by the sampling tube and the instrument were evaluated to be below 5 % by
 Loubet et al. (2022) and were neglected here. A footprint analysis for the whole campaign period was performed based
 on Kljun et al. (2015) and showed that at least 90 % of the total footprint contribution was always within the studied
 190 area (Fig. 1).

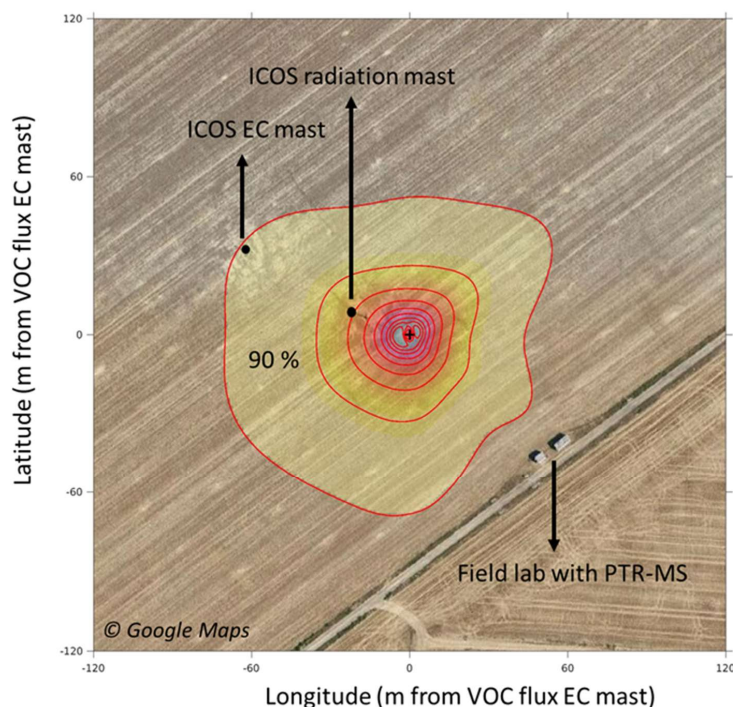


Figure 1: Flux footprint for the measurement campaign period (9 May – 30 June 2017) showing that at least 90 % of the flux contribution originates from the investigated rapeseed crop area (located north and north-west of the agricultural path appearing on this satellite picture). The black cross in the centre of the ellipses depicts the location of the eddy-covariance (EC) mast deployed in this study. The ICOS eddy covariance and radiation masts, and the field lab are also shown.

2.3 BVOC mixing ratio profiles and BVOC fluxes computation with the aerodynamic resistance approach

A BVOC mixing ratio profile was installed in the rapeseed field, comprising 5 lines positioned at 0.05 m, 0.25 m, 0.80 m, 1.55 m and 3 m above the ground, the rapeseed vegetation being 1.55 m height surrounding the mast. Every 30 minutes, each height was sequentially scanned by the PTR-Qi-TOF-MS for 1 minute using an 8 port 1/4" VICI valve. The air was drawn from each of these lines (1/4" external diameter, 1/8" internal diameter; 30 m length) with a Busch SV1010 pump at 6 NL min⁻¹ in each line using a flow splitter. The BVOC mixing ratio at each level was determined as the average mixing ratio over the last 30 s of sampling at this level. BVOC mixing ratio were calculated in the same way as explained at section 2.2.

The profile mixing ratio was further used to compute the flux based on the aerodynamic resistance approach using the two uppermost sampling heights (1.55 and 3.0 m), to serve as a diagnostic for the EC flux. Indeed, according to the resistance analogy the BVOC profile flux ($Profile_Flux_i$, nmol m⁻² s⁻¹) above the canopy is equal to the difference in mixing ratios divided by the aerodynamic resistance (Flechard et al. 2013). Acknowledging that the BVOC concentration is equal to the mixing ratio divided by the molar volume of air ($RT_a/\overline{p_a^d}$), we find:



$$210 \quad Profile_Flux_i = -\frac{C_i(3\ m) - C_i(1.55\ m)}{R_a(1.55\ m, 3\ m)} \times \frac{p_a^d}{R T_a} \quad (6)$$

Where $C_i(3\ m)$ and $C_i(1.55\ m)$ (ppb) are the BVOC mixing ratios measured at 3 m and 1.55 m height, and R_a ($s\ m^{-1}$) is the aerodynamic resistance which was approximated as $R_a(1.55\ m, 3\ m) \sim \frac{1}{k u_*} \ln\left(\frac{3-d}{1.55-d}\right) \sim \frac{1.02}{k u_*}$, with u_* being the friction velocity ($m\ s^{-1}$), d the displacement height (m), and κ the von Kármán constant (0.4), neglecting thermal stratification for simplification in this diagnostic approach. During the experiment the canopy height was 1.7 m height, the displacement height d and the roughness height z_0 were evaluated as 1.4 and 0.17 m respectively, where d was evaluated from Verhoef et al. (1997).

2.4 Ancillary data

Meteorological measurements were performed continuously at the FR-Gri site during the campaign following the ICOS standards. Among other variables, air temperature (T_{air}) and air humidity (RH) (HMP155a, VAISALA, Finland) at 1, 2.7 and 5 m heights, global incoming short-wave solar radiation at 5.3 m (model CNR4, Kipp & Zonen, Germany), and rainfall (model ARG100, Campbell, UK) were recorded.

CO₂ and H₂O fluxes were measured by eddy-covariance following the ICOS protocol (www.icos-ri.eu) using an enclosed path infrared gas analyser (model Li-7200, Li-COR, USA) and an ultrasonic anemometer (model HS-50, Gill Instruments Ltd, UK), located at around 50 m away from the BVOC mast. Crop height evolution was monitored at regular intervals. The leaf area index (LAI) and above-ground biomass were determined on three dates (11 November 2016, 16 March 2017 and 19 April 2017) with destructive samplings and planimeter measurements. The LAI was $5.2 \pm 1.5\ m_{leaf}^2\ m_{soil}^{-2}$ during the experiment (rapeseed plants were at their maximum leaf development when the experiment started), of which 80 % were leaves, and 20 % stems.

2.5 Data treatment and analysis

2.5.1 Selection of compounds with significant fluxes

In order to take into account, as much as possible, the possible variability of exchanged compounds over the whole measurement period (9 May - 30 June), we computed the 7-day running means of \bar{F}_i^h (\bar{F}_i^{7d}) and $\overline{R\bar{U}i^h}$ ($\overline{R\bar{U}i}^{7d}$) using the same quadratic averaging as in eq. (5) for $\overline{R\bar{U}i^h}$, and retained the BVOC for which $\bar{F}_i^{7d} > 3 \times \overline{R\bar{U}i}^{7d}$. By using moving windows, it was possible to detect singularities in the dataset. Finally, in order to apply this selection process to the whole measurement period, the selected BVOC were those which were retained by the above-mentioned criteria in 50 % of the dates. In the rest of the manuscript, the tentative name of each compound is used.

Iron-containing compounds identified as artefacts by Salazar Gómez et al. (2019) were withdrawn from the list of selected BVOC. Furthermore, the detected BVOC with a peak at m/z 63.006 could not be entirely distinguished from the m/z peak at 63.026 during the campaign, as a consequence of a wide peak integration definition around this m/z value; the identification of this compound is therefore uncertain: it could be dimethylsulfide (DMS) instead of methaneperoxy acid.

2.5.2 Defining sub-periods for data analysis and interpretation

Data analysis of the whole measurement period was separated into four sub-periods, in order to take account of (i) crop development stages and (ii) the observation of unusually large eddy-covariance deposition fluxes of some compounds during specific periods. First, as the vegetation was in continuous development during the measurement period, which is likely to have influenced the nature of exchanged BVOC, results interpretation was separated in two sub-periods: 9



May – 30 May, during which the vegetation was in the fruit development period (BBCH (Biologische Bundesanstalt, Bundessortenamt und Chemische Industrie) stages 70s, AHDB, 2023), and 9 – 30 June, during which the rapeseed crop entered and pursued senescence (BBCH stages 80s to 90s). Second, as unusually large deposition fluxes of certain
 250 BVOC species were observed with our eddy-covariance system – but not with the profile system (see further in the Results and Discussion sections) – over the periods 9-10 May and 23-30 May, it was decided to split the May data into three sub-periods so as to be able to better interpret the observed data. Therefore, eventually, the whole dataset was split into the four following sub-periods in the Results and Discussion sections:

- (1) Sub-period 1 (11 – 22 May 2017), representative of the rapeseed fruit development period
- 255 (2) Sub-period 2 (9 – 30 June 2017), representative of the rapeseed senescence period
- (3) Sub-period 3 (9 and 10 May 2017,) focusing on the first unusually large eddy-covariance deposition fluxes observed for some compounds
- (4) Sub-period 4 (22 – 30 May 2017), focusing on the second unusually large eddy-covariance deposition fluxes observed for some compounds

260 2.4.4 Calculation of Standard Emission Factors

As BVOC emissions by vegetation are driven by both temperature and light or solely by temperature, these emissions can be normalised by light and temperature functions to produce standardised emission factors (SEF), which are helpful for comparison with previous studies. The SEF were calculated for sub-periods 1 and 2 (see section 2.5.2) based on Guenther et al. (1995) and Guenther (1997) as described by Gonzaga Gomez et al. (2019). For fluxes depending on
 265 light and temperature, such as isoprene, the SEF for each compound i ($\mu\text{g m}^{-2} \text{h}^{-1}$) is defined by:

$$SEF_i = \frac{E_i}{C_L C_T} \quad (7)$$

Where E_i is the measured BVOC flux per leaf surface ($\mu\text{g m}^{-2} \text{h}^{-1}$), and C_L and C_T are the temperature and light response function of the BVOC emissions, defined as:

$$C_T = \frac{\exp\left[\frac{C_{T1}(T-T_S)}{R T_S T}\right]}{1 + \exp\left[\frac{C_{T2}(T-T_M)}{R T_S T}\right]} \quad \text{and} \quad C_L = \frac{\alpha C_{L1} L}{\sqrt{1 + \alpha^2 L^2}} \quad (8)$$

270 Where $C_{T1} = 95000 \text{ J mol}^{-1}$, $C_{T2} = 230000 \text{ J mol}^{-1}$, $T_M = 314 \text{ K}$, $\alpha = 0.0027$, $C_{L1} = 1.066$ are empirically derived constants, T is the leaf experimental temperature (K), T_S is the leaf temperature at standard condition (303 K), R the gas law constant ($8.314 \text{ J mol}^{-1} \text{ K}^{-1}$), and L is the photosynthetically active radiation (PAR) flux ($\mu\text{mol photon m}^{-2} \text{ s}^{-1}$).

For BVOC emissions depending only on temperature (e.g. monoterpenes), the SEF was determined using the following equation (Eq. 9) with the empirical constant β set to 0.09 K^{-1} :

$$275 \quad SEF_i = \frac{E_i}{\exp(\beta(T-T_S)) \exp(\beta(T-T_S))} \quad (9)$$

To compute the SEF, the BVOC flux per leaf surface, E_i ($\mu\text{g m}^{-2} \text{h}^{-1}$), was computed from the molar flux \bar{F}_i^h ($\text{nmol m}^{-2} \text{ s}^{-1}$), the molar mass M_i (g mol^{-1}) of compound i , and the leaf area index (LAI, $\text{m}^2 \text{ m}^{-2}$) as:

$$E_i = \frac{3600}{1000} \times \frac{M_i}{LAI} \times \bar{F}_i^h \quad (10)$$



280 Where the ratio 3600/1000 converts seconds to hours and ng to μg . It should be noticed that the SEF computed in this study represent the ecosystem and not the plants alone since the eddy-covariance fluxes integrate over the whole ecosystem.

The SEF calculated for all the compounds showing a significant emission for both sub-periods 1 (fruit development period) and 2 (senescence period) were compared to values taken from three references: i) the MEGAN2.1 model (Guenther et al., 2012), ii) the study by Havermann et al. (2022) and iii) the study by Gonzaga Gomez et al. (2019):

285 MEGAN2.1 is a widely used model that provides estimates of BVOC flux exchanges between the terrestrial biosphere and the atmosphere. This model categorises ecosystems between 15 plant functional types (PFT) and does not distinguish between crop species as they all fall into a unique category (PFT 15). Additionally, bare soil is considered to have null BVOC emissions. The model also categorises BVOC into individual (e.g. methanol, isoprene, acetone) and compound classes (bidirectional BVOC, stress BVOC, etc.) according to chemical characteristics. Although we did not strictly use the same model as MEGAN2.1 to compute the SEF from the measured fluxes, the equations are comparable
290 in Guenther et al. (1995) and MEGAN2.1.

Havermann et al. (2022) measured BVOC fluxes using large chambers deployed on three crop species (maize, rapeseed and ryegrass). They then calculated the SEF based on empirical light- and temperature-dependent relationships. Since they report SEF on a dry weight basis, we divided their SEF by the leaf specific area for rapeseed they report (39.6
295 $\text{m}^2 \text{kg}^{-1}$) to retrieve the SEF per unit leaf area. It has to be noted that the leaf specific area measured in the present study is $20 \pm 1 \text{ m}^2 \text{kg}^{-1}$, which is half of what is reported by Havermann et al. (2022).

Gonzaga Gomez et al. (2019) measured BVOC fluxes using dynamic automated chambers deployed on rapeseed, wheat and maize at the same site and field campaign as the one reported in the present study. They calculated the SEF based on the empirical light- and temperature-dependent relationships from Guenther et al. (1995).

300 2.4.5 Calculation of the OH reactivity flux

The total OH reactivity R (s^{-1}) is usually calculated as Eq. 11 (Gros and Zannoni, 2022):

$$R = \sum_i k_{OH+i} \times N_{avo} \times \frac{P}{R \times T} \times 10^{-1} \times C_i \quad (11)$$

Where k_{OH+i} ($\text{cm}^3 \text{molecule}^{-1} \text{s}^{-1}$) is the rate constant of the reaction between OH and BVOC i (Table 2 and references therein), N_{avo} ($6.022 \times 10^{23} \text{ molecule mol}^{-1}$) is the Avogadro number, P (101325 Pa) is the atmospheric pressure, R (8.314
305 $\text{J K}^{-1} \text{mol}^{-1}$) is the gas law constant, T (298 K) is the air temperature, 10^{-15} is a conversion factor, and C_i (nmol mol^{-1}) is the mixing ratio of BVOC i .

To compare the OH reactivity resulting from the SEF found in this study to those resulting from literature emission factors, we computed a standard OH reactivity flux (here indicated as RF). It is representative of a total net OH reactivity that would result from the emitted BVOC. It was computed as Eq. 12:

$$310 \quad RF = \sum_i k_{OH+i} \times N_{avo} \times \frac{P}{R \times T} \times 10^{-1} \times \left(SEF_i \times V_{mol}^{air} \times \frac{LAI}{M_i} \times \frac{1000}{3600} \right) \quad (12)$$

Where SEF_i in $\mu\text{g m}^{-2} \text{h}^{-1}$ is the standard emission factor of BVOC i , and the term on the right side of the equation is needed to transform the SEF unit into $\text{nmol mol}^{-1} \text{m s}^{-1}$, which leads to RF being in m s^{-2} , that is the unit of the OH reactivity (s^{-1}) multiplied by an exchange velocity (m s^{-1}). V_{mol}^{air} ($\text{m}^3 \text{mol}^{-1}$) is the air molar volume, M_i (g mol^{-1}) is the molar mass of BVOC i and LAI is the leaf area index ($\text{m}^2 \text{m}^{-2}$).

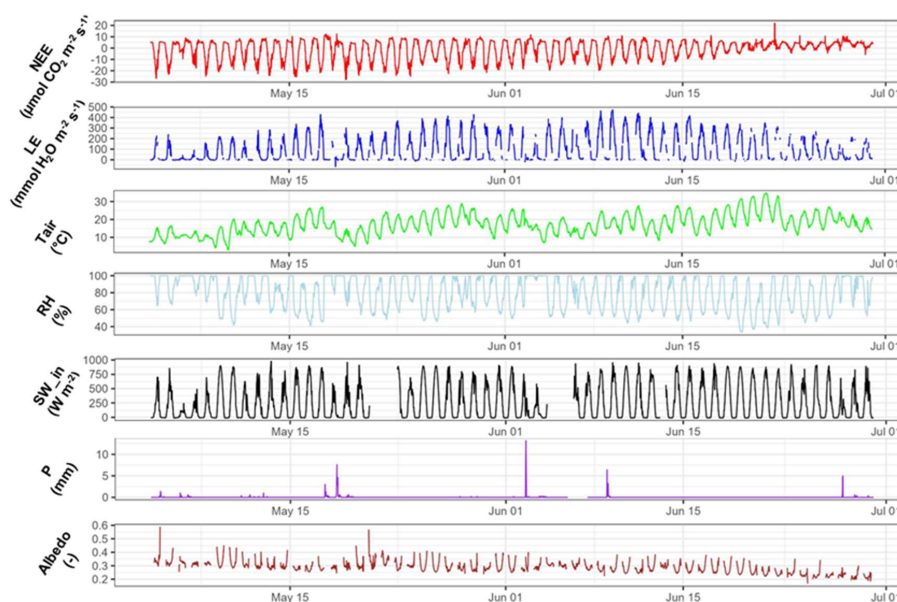


315 In this study, we used the OH reactivity flux to compare the impact of BVOC SEF computed here with the SEF available from the model MEGAN 2.1. To do that, only the compounds with a SEF explicitly reported in MEGAN 2.1 were used in this calculation.

3 Results

3.1 Meteorological conditions and crop development

320 The BVOC flux measurement campaign started as rapeseed was already in the fruit development phase and actively photosynthesising, as shown by the Net Ecosystem Exchange (NEE) fluxes being largely negative during daytime (Fig. 2). The investigated period was also characterised by significant evaporation (latent heat, LE, Fig. 2) during the whole time. As of June, gradual decreases in the CO₂ flux (from about -20 to 0 μmol m⁻² s⁻¹) and in the albedo (from about 0.35 to 0.25) were observed as a consequence of progressive crop senescence, while evaporation was sustained. The air temperature was variable during the whole measurement period, and comprised between 2.9 and 34.7 °C, with an average value of 16.9 °C. A few short rain events punctuated the measurement period, especially around mid-May and early June.



330 **Figure 2: CO₂, H₂O fluxes and meteorological conditions during the field campaign: net ecosystem exchange (NEE), latent heat (LE), air temperature (T_{air}), relative humidity (RH), short-wave incoming radiation (SW_{in}), precipitation (P) and Albedo (ratio).**

3.2 Eddy-Covariance ecosystem BVOC fluxes during fruit development and senescence

335 Out of more than 500 detected ions, 42 BVOC (corresponding to 62 ions when including isotopes and fragments), exhibited significant fluxes (Table 1 for the list of the twenty most exchanged BVOCs during sub-periods 1 and 2, and Table S03 and Fig. S04 for the whole list and flux (black) + random error (red) temporal courses of the 42 BVOC, respectively). Overall, 30 BVOC were emitted, 7 were deposited, and 5 were bidirectional (Table S03).

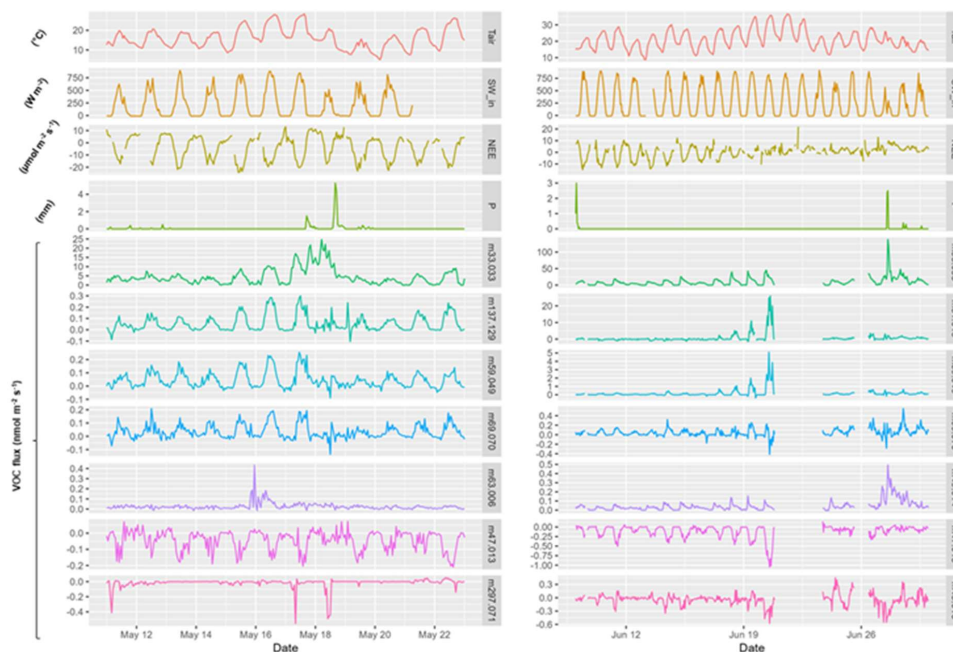


340 Among the emitted BVOC, m/z 33.033 (methanol) was by far the most emitted one for both sub-periods (Tables 1 and S03, Fig. 3), representing between 90 and 93 % of the total emissions on a molar basis (Table 1). The magnitude of methanol emissions was twice larger during the senescent sub-period than during the end of fruit development period (Table 1, Fig. 3). The other three most emitted BVOC were m/z 137.129 (monoterpenes), m/z 59.049 (acetone) and m/z 69.070 (isoprene) in the fruit development sub-period, and m/z 31.018 (formaldehyde), m/z 59.049 (acetone) and m/z 49.014 (methanethiol) in the senescence sub-period, with these compounds representing between 0.4 and 5.8 % of emissions (on a molar basis) during these two respective sub-periods (Table 1).

Table 1: Twenty most net emitted and net deposited compounds during sub-periods 1 and 2. The proportions (Prop. (%)) of net emissions/depositions for each compound with respect to the total fluxes are indicated separately for each period.

m/z	Molecular formula	Tentative compound name	Net emitted (E) or net deposited (D) ^a	Sub-period 1: 11 - 22 May End of the flowering period		Sub-period 2: 9 - 30 June Senescence period	
				Prop. ^b (%)	Mean Flux ^c (nmol m ⁻² s ⁻¹)	Prop. (%)	Mean Flux (nmol m ⁻² s ⁻¹)
		Total emission flux (over all significant compounds)	na	4.82 (0.028)	na	11.54 (0.027)	
		Total deposition flux (over all significant compounds)	na	-0.09 (0.005)	na	-0.24 (0.007)	
31.018	(CH ₂ O) ⁺	Formaldehyde; hydroxymethylene †	D, E	12.8 -0.011 (0.005)	5.8	0.667 (0.005)	
33.033	(CH ₄ O) ⁺	Methanol †	E	92.7 4.46 (0.007)	89.8	10.35 (0.006)	
41.038	(C ₃ H ₄) ⁺	Fragment of a variety of compounds ‡	E	0.3 0.014 (0.023)	0.3	0.039 (0.022)	
43.018	(C ₂ H ₂ O) ⁺	Methylvinylketone, fragments of several oxygenated compounds ‡; Hexyl acetate fragment ‡	E, D	0.3 0.017 (0.0007)	16.9	-0.040 (0.0007)	
45.033	(C ₂ H ₄ O) ⁺	Acetaldehyde, Ethylene oxide†	E	0.3 0.015 *	0.3	0.035 *	
47.013	(CH ₂ O) ₂ ⁺	Formic acid†	D	50.3 -0.044 (0.0002)	44.9	-0.107 (0.0002)	
49.014	(CH ₃ S) ⁺	Methanethiol†; Hydroxylamine, Ethyl ‡	E	0.3 0.016 (0.0002)	0.4	0.046 (0.0002)	
51.022	(C ₄ H ₂) ⁺	Diacetylene, 1,3-Butadiene †	E	0.1 0.004 (0.01)	0.1	0.009 (0.01)	
59.049	(C ₃ H ₆ O) ⁺	Acetone (propanal) and/or methyl vinyl ether (MVE) † ‡	E	0.9 0.044 (0.0003)	1.5	0.169 (0.0003)	
60.048	(C ₂ H ₃ NO) ⁺	Acetamide, formamide N-methyl-, nitrosoethane ‡	E	0.1 0.004 (0.0003)	0.1	0.012 (0.0003)	
61.029	(C ₂ H ₄ O ₂) ⁺	Acetic acid and glycolaldehyde ‡	E, D	0.3 0.015 (0.007)	15.1	-0.036 (0.007)	
62.029	(CH ₃ NO ₂) ⁺	Nitromethane; methylnitrite ‡	E	0.1 0.007 (0.0004)	0.1	0.009 (0.0004)	
63.006	(CH ₂ O) ₃ ⁺	Fragment ‡ or possibly Dimethylsulfide † (m/z 63.026) if the peak integration was not good	E	0.5 0.026 (0.005)	0.3	0.035 (0.005)	
69.070	(C ₃ H ₈) ⁺	Isoprene†	E	0.7 0.035 (0.002)	0.4	0.048 (0.002)	
73.064	(C ₄ H ₈ O) ⁺	Methyl-ethyl-ketone (MEK), ethyl-vinyl-ether, butanal, 2-butanone ‡; MEK, propanal 2-methyl ‡	E	0.2 0.008 (0.0008)	0.1	0.013 (0.0005)	
93.035	(C ₃ H ₈ O ₂) ⁺ ; (CH ₃) ₂ SiOH(H ₂ O) ⁺	2-Methylmercaptoethanol †; Trimethylsilanol H ₂ O cluster ‡	E	0.2 0.010 (0.0005)	0.1	0.008 (0.0005)	
105.066	(C ₈ H ₈) ⁺	Styrene, Olefin† ‡ †	E	0.3 0.016 (0.002)	0.0	0.0008 *	
137.129	(C ₁₀ H ₁₀) ⁺	Monoterpenes†	E	1.1 0.055 (0.0001)	0.3	0.036 (0.0001)	
223.057	(C ₆ H ₁₈ O ₃ Si ₃) ⁺	D3-siloxane Hexamethylcyclotrisiloxane ‡ ‡ §	D	14.0 -0.012 *	14.8	-0.035 *	
297.071	(C ₈ H ₂₄ Si ₄ O ₃) ⁺	D4-siloxane Octamethylcyclotetrasiloxane ‡ ‡	D	18.8 -0.017 *	2.5	-0.006 *	

^a Net emitter (E) or deposited (D) characteristic is evaluated over each single sub-period, e.g. D/E denotes that this BVOC was seen to deposit in May, then to be emitted in June. ^b Proportions were calculated within each net deposited or emitted group of compounds for each respective period. ^c Error is calculated as the root of the sum of squares of data over each respective period. ^(*) Error is lower than 0.001. "na" means "not applicable". References for compound identification: † Yáñez-Serrano et al., 2021 (GLOVOC database); ‡ Salazar-Gomez et al., 2019; # Chen et al., 2022; § Holzinger et al., 2019. In this table, the total for both net emitters and net depositors does not reach precisely 100% as this was established based on the 42 significant compounds (complete list in Table S01). Ta_mean = 18.1 °C and SW_in_mean = 276.4 W m⁻² during sub-period 1, and Ta_mean = 19.1 °C and SW_in_mean = 281.5 W m⁻² during sub-period 2, with Ta_mean being the average air temperature and SW_in_mean being the incoming total radiation.



380 **Figure 3: Air temperature (T_{air}), short wave incoming radiation (SW_in), net ecosystem exchange (NEE), Precipitation (P), and BVOC exchanged fluxes of a selection of 4 most emitted and 2 most deposited BVOC over sub-period 1 (left) and 2 (right). BVOC are named after their m/z ratio, on the right-hand side of each graph (see Table 1 for correspondence. Units of each variable are given on the left-hand side of the graphs.**

385 Along these main compounds, many other BVOCs belonging to different chemical compound classes were observed to be emitted and tentatively identified (Table S03). (i) Two other **terpenoid compounds** than isoprene and monoterpenes was seen to be significantly emitted during sub-periods 1 and 2 (Fig. S04): methylbutenol (MBO, m/z 87.078) and sesquiterpenes (m/z 205.186), which both exhibited much clearer fluxes – even if rather small compared to methanol – during the fruit development period than during the senescence period. (ii) Possible other **sulphur compounds** than methanethiol (m/z 49.014) were also emitted in significant amounts during both

390 sub-periods 1 and 2: m/z 63.006 (which could actually be m/z 63.026, identified as dimethylsulfide, see section 2.5.1), m/z 75.025, possibly identified as methyl-vinyl sulfide, m/z 93.035, possibly identified as 2-methylmercaptoethanol but which could also be $(C_6H_4O)H^+$ (unidentified ion), and m/z 95.015, possibly identified as dimethyl sulfone. (iii) **BVOCs likely containing nitrogen** were also seen to be emitted, with clear diurnal patterns over the whole measurement campaign (m/z 60.048, possibly identified as acetamide, and m/z 62.029,

395 possibly identified as nitromethane, and clear diurnal pattern particularly during sub-period 1 (m/z 118.074, which could be indole, a quite reactive compound). (iv) Many **oxygenated compounds** were also seen to be emitted during both sub-periods, though at much smaller rates than methanol: acetaldehyde (m/z 45.033), m/z 73.064 (possibly identified as methyl-ethyl-ketone (MEK, butanone), or butanal, or ethyl-vinyl-ether), m/z 83.049 (possibly identified as hexanal fragment or methylfuran), m/z 87.042, m/z 87.078, m/z 101.059 (possibly identified as pentanedial or other compounds), and m/z 115.078 for which proposed compounds are hexenoic acid or

400



caprolactone (Table S03). (v) **Hydrocarbons** were also observed: m/z 67.053 (1,3-cyclopentadiene), m/z 83.084 (cyclohexene), and m/z 105.066 (possibly styrene).

A few compounds were seen to be deposited (Fig. 3, Fig. S04) during sub-periods 1 and 2: they are formic acid (m/z 47.013), which represented about 45-50 % of the deposited BVOC flux in each sub-period, m/z 77.005, possibly identified as thioacetic acid, m/z 99.008, possibly identified as maleic anhydride, and much heavier compounds like m/z 223.057, m/z 297.071 and m/z 355.051 possibly identified as D3-siloxane, D4-siloxane and D5-fragment of siloxane compounds, respectively.

Some BVOC switched from deposition to emission, or vice-versa, between sub-periods. One BVOC (formaldehyde, m/z 31.018) was seen to be deposited in small amounts during sub-period 1, then switched to emissions during sub-period 2. The quantification of formaldehyde fluxes should be considered with caution due to its proton affinity (712.9 kJmol^{-1} ; NIST database, 2023) being close to that of water (691 kJmol^{-1} ; NIST database, 2023), potentially making it more difficult to detect it using the PTR-MS technique adequately (Loubet et al., 2022). Conversely, three BVOC (m/z 57.069 (possibly butene), m/z 61.029 (identified as acetic acid) and m/z 167.052 (possibly identified as thiocresol)) were emitted during the end of the flowering period, then deposited during the senescence period (Table 1, Fig. S04).

All the detected compounds exhibited diel emission or deposition patterns during both sub-periods (Fig. 3 and S04). BVOC fluxes increased (in absolute value) during the day and decreased to lower nocturnal emission rates following radiation and temperature variations. During sub-period 1, a rain event occurring between the 17th and 18th of May, together with a temperature drop, likely caused reductions in all the detected BVOC emission rates (Fig. 2, 3 and S04). Formaldehyde and formic acid deposition rates were also reduced during that specific event. The short rain events during sub-period 2 did not decrease BVOC emissions, probably because rain intensity was smaller than in sub-period 1 and air temperatures remained high. During sub-period 2, a temperature increase that started around mid-June, together with bright sun conditions, could have triggered larger fluxes for the majority of BVOC (Fig. 3, Fig. S04).

As observed in Fig. 3 and in Fig. 4 (panels A, B and C), most BVOC fluxes peaked around noon. However, a few BVOC exhibited a maximum flux during the morning, followed by a decrease during the rest of the day. This was the case for methanol, m/z 63.006 and formic acid during sub-period 1, and for methanol, methanethiol and acetic acid during sub-period 2. During sub-period 1, NEE flux and radiation also peaked earlier than noon (Fig. 4, panels D and E), while this was not the case in the second sub-period. Concerning nocturnal emissions of methanol, we noticed smaller (about 50 %) emission fluxes during senescence compared to the end of flowering period, while diurnal emissions of this compound were more than twice larger during senescence compared to end of flowering.

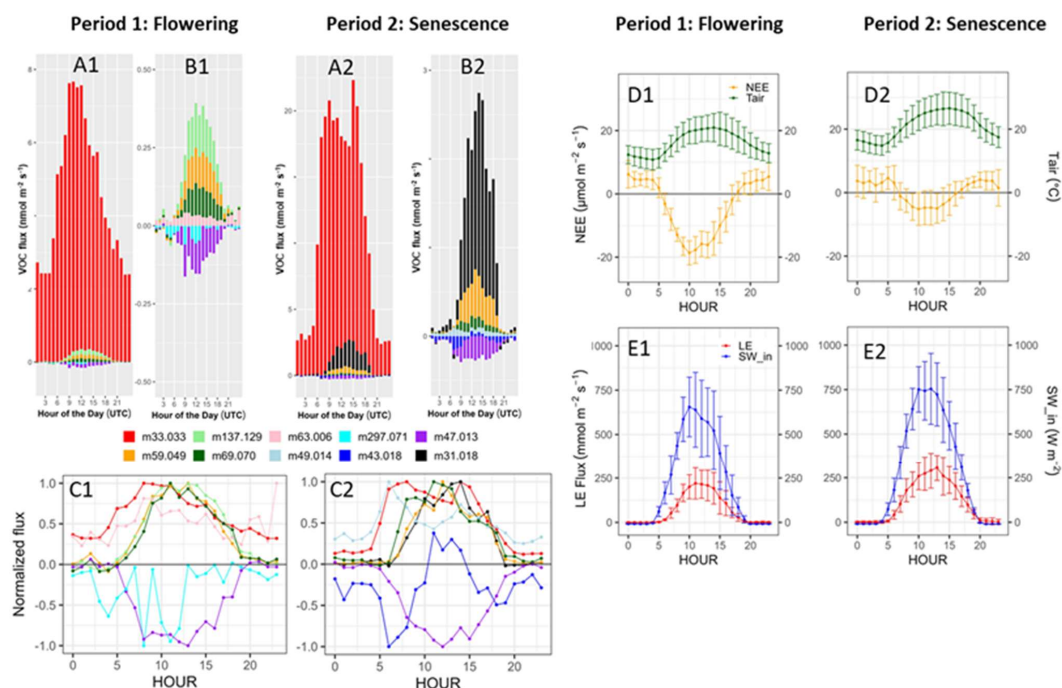


Figure 4: Diel cycles of main BVOC fluxes and micro-meteorological variables during sub-periods 1 and 2:

435 **A, stacked hourly BVOC fluxes ($\text{nmol m}^{-2} \text{s}^{-1}$) for the 10 most emitted and deposited BVOC; B, same as A, without methanol (m/z 33.033); C, BVOC fluxes divided by their daily maximum; D, net CO_2 fluxes (NEE) and Air temperature (T_{air}); E, latent heat fluxes (LE) and global incoming radiation (SW_in). Index 1 refers to sub-period 1 (fruit development), and index 2 refers to sub-period 2 (senescence).**

3.3 Emission factors and OH reactivity fluxes

440 The calculated standard emission factors (SEF) showed much larger values for methanol than for other oxygenated BVOCs like acetone, formaldehyde, acetaldehyde, and for terpenoid compounds (isoprene, monoterpenes, MBO, sesquiterpenes) (Table 2). Generally, SEF values were of similar magnitude or reduced during sub-period 2 as compared to sub-period 1 (reduction factors varying from 1.2 (acetaldehyde) to about 20 (sesquiterpenes and indole). Only methanol and acetone – and to a smaller extent m/z 101.059 – SEFs were increased from sub-period 445 1 to sub-period 2, by factors between 1.2 and 2.8.

Compared to values taken into consideration in the MEGAN2.1 model (Guenther et al., 2012), the SEFs calculated in the present study exhibited values $\sim 35\%$, 3 times and 10 times smaller for methanol, acetone and acetaldehyde, respectively, on average over both sub-periods. On the contrary, they were in the same range (acetaldehyde) or 2.5 (acetone) to 3.5 (methanol) times larger than values reported by Havermann et al. (2022). Also, much smaller SEF values than in MEGAN2.1 were reported in the present study for more reactive compounds like indole, methanethiol and m/z 101.059. On the other side, much larger SEF values for monoterpenes (10 times, during the fruit development period), isoprene (13 and 6.5 vs 1, during both sub-periods, respectively), MBO (10 to 200 times) and formaldehyde (25% larger) were observed in the present study, compared to those in MEGAN2.1. The isoprene and monoterpenes SEFs reported in the present study was also generally larger, or in the same range of values, as compared to SEFs reported by Gonzaga Gomez et al. (2019) and Havermann et al. (2022).

455



The OH reactivity fluxes (RF) computed using MEGAN2.1 SEF or this study SEF were differing in the same way as the SEF with smaller MEGAN2.1 OH reactivity flux for isoprene, MBO, monoterpenes and formaldehyde, and larger MEGAN2.1 OH reactivity flux for methanol, acetone, sesquiterpenes, acetaldehyde, indole, methanethiol and m/z 101.059, as compared to the SEFs calculated in the present study (Table 2). In order not to introduce a large disequilibrium due to uncertain SEF on these last three compounds, we chose not to include these compounds in the evaluations of the total OH reactivity flux and the contributions of each compound to this total amount. In terms of BVOC contribution to the total OH reactivity flux, formaldehyde dominated and contributed in similar proportions to what can be evaluated with MEGAN2.1 SEFs. Contribution of monoterpenes to the total OH reactivity flux was then seen to be much larger (more than 8 times) based on results from the present study as compared to results obtained with MEGAN2.1 evaluation, for which contributions are mainly shared in the same range (27-33 %) by other BVOC like methanol, formaldehyde and acetaldehyde. In our study, the contribution of methanol, in particular, to total OH reactivity flux was actually seen to be about half what is evaluated with MEGAN2.1 SEF.



Table 2: Standard emission factors (SEF), OH reactivity flux and BVOC contribution to OH reactivity flux calculated in the present study for both crop development sub-periods, compared with values from previous studies, either obtained from experimental or modelling works. P1 represents the fruit development crop stage, and P2 corresponds to the senescence period.

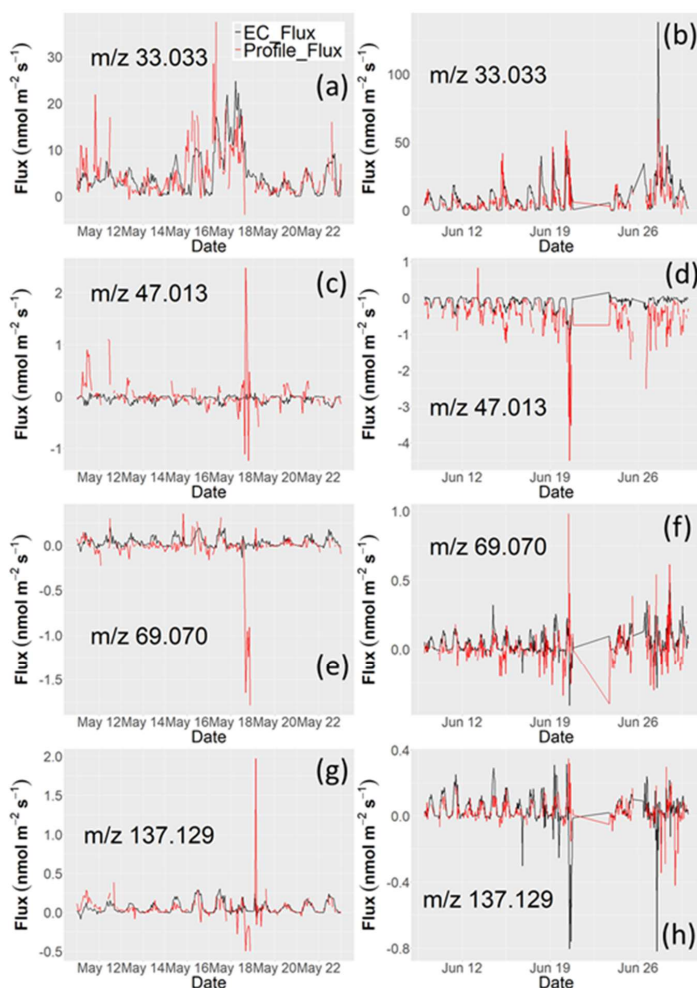
m/z	Tentative VOC identification		SEF [$\mu\text{g m}^{-2}$ (leaf) h^{-1}]			OH reactivity constant ($\text{cm}^3 \text{ molecules}^{-1} \text{ s}^{-1}$)	OH reactivity flux [m s^{-2}]		Contribution (%) to total OH reactivity		
	Ion formulas	VOC names	This study ^a	MEGAN2.1 ^b	G2021 ^c		H2022 ^d	This study	MEGAN2.1	This study	MEGAN2.1
			P1	P2			P1-P2		P1-P2		
	Oxygenated and terpenes VOC										
33.033	(CH4O)H+	methanol	485	641	na	150	1.22E-02	1.95E-02	18.42%	30.89%	
59.049	(C3H6O)H+	acetone	13.9	39.2	na	11	6.46E-05	1.94E-04	0.10%	0.31%	
69.070	(C5H8)H+	isoprene	13.1	6.5	12-18	11	1.13E-02	1.15E-03	17.06%	1.82%	
87.078	(C5H10O)H+	MBO	2	0.3	na	na	6.30E-11 (@)	5.77E-06	1.03%	0.01%	
137.129	(C10H16)H+	monoterpenes	40	7	0.3 - 5	14	1.24E-10 (c)	1.69E-02	25.48%	3.01%	
205.186	(C15H24)H+	sesquiterpenes	3	0.2	2 - 4	na	1.50E-10 (c)	9.88E-04	1.49%	2.76%	
	Bi-directional VOC										
31.018	(CH2O)H+	formaldehyde	na	102	na	na	2.23E-02	1.75E-02	33.60%	27.62%	
45.033	(C2H4O)H+	acetaldehyde	8	6	na	5.5	1.87E-03	2.12E-02	2.82%	33.57%	
	Stress VOC										
118.078	(C8H7N)H+	indole	0.9	0.04	na	na	4.85E-04	3.12E-01	na	na	
	Other VOC leaf surface compounds										
49.014	(CH4S)H+	methanethiol	2.6	1.4	na	na	1.08E-03	7.51E-02	na	na	
101.059	(C5H8O2)H+	4-oxopentanal (4-OPA)	2.4	2.8	na	na	4.06E-04	2.21E-02	na	na	
			Summed reactivity flux ^f				0.067	0.063	100%	100%	

a SEF calculated with the equation proposed by (Guenther et al., 1995; Guenther, 1997), depending on both temperature and radiation. b Values from Guenther et al. (2012). c Values from Gomez et al. (2021). d Values from Havermann et al. (2022), considering a rapeseed biomass density of 1100 g m^{-2} and a leaf specific area of $39.6 \text{ m}^2 \text{ kg}^{-1}$. e Categories from MEGAN2.1 model (Guenther et al. (2012). f summed reactivity not accounting for "stress BVOC" and "other BVOC leaf surface compounds". (@) Values from IUPAC standard reference base (<https://iupac-aeris.inrs.fr/>). 2023. (*) Values from Atkinson et al. (1995). (\$) Value from Fruetilde et al. (1998). "na" means that no data were available (for formaldehyde in P1, no emission data was available as this compound was seen to be deposited).



3.4 Fluxes by aerodynamic resistance approach during sub-periods 1 and 2

480 Fluxes measured either by the eddy-covariance method (EC_Flux) or by the aerodynamic resistance approach (Profile_Flux) were generally in good agreement for emission behaviours, as for example for methanol and monoterpenes over the periods 11-22 May (Fig. 5 and Fig. S05b) and 9-30 June (Fig. 5 and Fig. S05d). Differences in magnitude were however observed for deposited compounds over the period 9-30 June (Fig. 5 and Fig. S05d), with Profile_Flux being larger e.g. for formic acid (m/z 47.013) and acetic acid (m/z 61.029). For some compounds
 485 (m/z 75.025, 115.078), the flux direction is even different between both estimations over the period from 9 to 30 June (Fig. S05d), with emission observed by the EC method and deposition observed with the aerodynamic resistance approach. Such differences were not observed during sub-period 1 (Fig. S05b).



490 **Figure 5: Comparison of BVOC fluxes measured by eddy-covariance (black lines) or with the aerodynamic resistance approach (red lines) for four BVOC during both flowering (sub-period 1) and senescence (sub-period 2) vegetation stages. a and b: methanol (m/z 33.033). c and d: formic acid (m/z 47.013). e and f: isoprene (m/z 69.070). g and h: monoterpenes (m/z 137.129).**

3.5 Identification of potential fast gas-phase chemical reactions for BVOC at the site

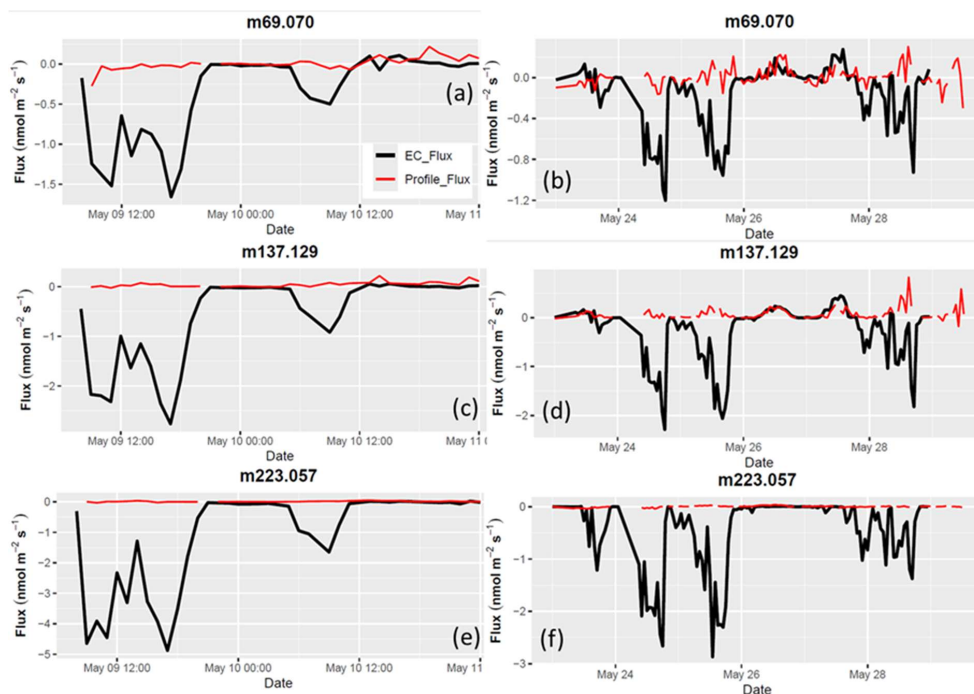


We observed that, most of the time, mixing ratios were in good agreement between EC and profile measurement systems sampling at the same height of 3 m, for the majority of compounds during all four sub-periods (Fig. S05a-d). However, during sub-periods 3 (9-10 May), and 4 (23-30 May), the mixing ratios were up to 15 times higher in the EC line, indicating a very strong gas-phase reaction occurring for some BVOC, and in particular terpenes and siloxanes during these periods, combined with high mixing ratios of these compounds (Fig. S05a and S05c).

The reason for these differences may be due to chemical reactions in the gas-phase occurring during the transport in the tubes. Indeed, given the difference in inlet lines length and flow rates in those lines, the transport time was $t_{EC} = 3.6$ s in the EC set-up and $t_{profile} = 11.3$ s in the profile set-up. This led to BVOC being either consumed or produced in differing amounts in the two tubing systems. Assuming a first-order reaction with a non-limiting reactant mixing ratio, the reaction constant of a compound i in the atmosphere $k_{atm,i}$ (s^{-1}) could be computed as $k_{atm,i} = \ln(C_{EC} / C_{profile}) / (t_{profile} - t_{EC})$, with $t_{profile} - t_{EC} = 7.7$ s.

We find reaction rates varying up to 0.04 s^{-1} , 0.12 s^{-1} and 0.25 s^{-1} during the sub-periods 3 and 4 for isoprene, monoterpenes and D3-siloxane, respectively (see Fig. S09 for reaction rates for all compounds during the experiment).

We also observed during these sub-periods 3 and 4, that some BVOC, and in particular, monoterpenes, isoprene, siloxanes, exhibited large eddy-covariance deposition fluxes that followed a diel pattern (Fig. 6, S05a and S05c).



510

Figure 6: Fluxes of isoprene (m/z 69.070, a), monoterpenes (m/z 137.129) and D3-siloxanes (m/z 223.057) measured with the eddy-covariance (black curves) and the aerodynamic resistance approach (red curves) during sub-periods 3 (a, c, e) and 4 (b, d, f).

For monoterpenes, these deposition fluxes reached about 10 times the magnitude of emitted fluxes for the same compounds during sub-periods 1 and 2, and deposition velocities (V_d , m s^{-1}) were far above the maximum exchange deposition velocity (V_{max} , m s^{-1}) indicating clearly a gas phase reaction mechanism to explain the observed apparent deposition velocity (Fig. S06a for isoprene and Fig. S06b for monoterpenes). During these



episodes, we further observed that the compounds exhibiting large EC deposition fluxes showed a mixing ratio much larger (and variable) in the EC setup than in the profile setup at the same sampling height of 3 m. This was in particular true for siloxane compounds (D3-siloxane, m/z 223.057 and isotopes, and D4-siloxane, m/z 297.071 and isotopes + fragments), and terpenes for all four sub-periods. Furthermore, during these periods, the fluxes computed with the aerodynamic resistance approach for these compounds showed no or slight deposition when compared to the large EC deposition fluxes, even for BVOC that are usually seen to be deposited like formic acid or acetic acid (Fig. 6, and S05a).

To investigate the origin of these atypical fluxes, meteorological conditions during sub-periods 3 and 4 were looked into details. While no atypical events were observed for rain, air humidity or air temperature (Fig. 2), wind direction was always in the North-East sector (0 – 100 deg/N, Fig. S07). Polar plots of BVOC mixing ratios measured in the eddy-covariance line (Conc_EC) over the whole measurement campaign, showed that those BVOC showing atypically large deposition in sub-periods 3 and 4, showed peaking mixing ratios with wind from the north-east sector, which strongly suggests a local source of these compounds in that direction (Fig. 7 and S08). We further see in Fig. 7 that for monoterpenes (m/z 137.129) and D3-siloxane (m/z 223.057) the concentration increases for wind speeds above a certain threshold ($\sim 1 \text{ m s}^{-1}$ for D3-siloxane), indicating advection from a local source of a highly reacting compound.

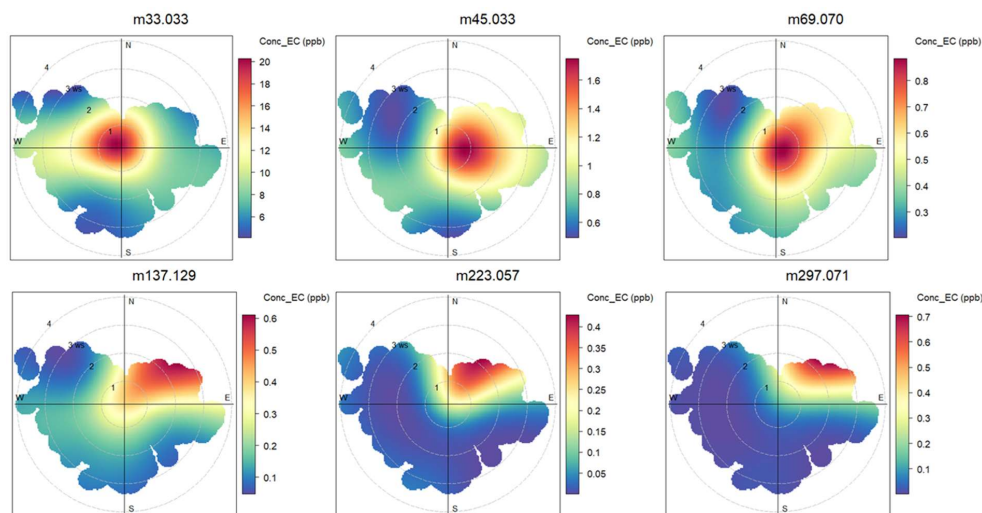


Figure 7: Polar plots of the mixing ratios of six selected BVOC, as measured by the eddy-covariance set-up over the whole measurement campaign (9 May – 30 June). The radius variable is the wind speed. The first row shows compounds that do not exhibit atypical fluxes in subperiods 3 and 4 (m/z 33.033, m/z 45.033 and to a lesser extent m/z 69.070) while the second row shows such compounds (m/z 137.129, m/z 223.057 and m/z 297.071). The complete set of polar plots for all significant BVOC in this study is displayed in Fig. S08 in the Supplementary Material.

4 Discussion

4.1 Dominance of methanol emissions at the ecosystem scale

In the present study, which is, to our knowledge, the first one applying the eddy-covariance technique to measure BVOC fluxes over a rapeseed crop, methanol was found to have the largest fluxes of all measured BVOC, and its contribution varied between 90 and 93 % of the summed BVOC emitted fluxes on a molar basis. This compound is known to be produced during plant growth and cell wall elongation (Fall and Benson, 1996). The prevalence of



methanol emissions from vegetated ecosystems (generally at least 50 % of emissions), and particularly from crops, is well known and was reported in several studies for other crops than rapeseed (for maize, see Bachy et al. (2016), Das et al. (2003), Graus et al. (2013), Wiß et al. (2017); for winter wheat see Bachy et al. (2018, 2020), Gonzaga Gomez et al. (2019), Loubet et al. (2022); for grasslands see Ruuskanen et al. (2011)). The dominant methanol contribution observed in this work agrees with previous studies by Gonzaga Gomez et al. (2019) and Havermann et al. (2022), both performed using automated dynamic chambers deployed on rapeseed plants in the field, but shows larger proportions. In particular, Gonzaga Gomez et al. (2019), carried out measurement with two cuvettes during the same campaign showing methanol contributing from 56 to 77 % of the summed molar BVOC emissions, while Havermann et al. (2022) reported a contribution of more than 80 %. Since these studies were carried out with chambers, either not including (Gonzaga Gomez et al., 2019) or including (Havermann et al. 2022) soil, this difference suggests that the share of methanol emissions from the soil would be larger than from the vegetation. In a lab experiment conducted with rapeseed plants, Voyard et al. (2024) also reported a large contribution (between 30 and 90 %) of methanol to total emissions, both from above-ground and below-ground plant parts.

In absolute values, the methanol emissions observed in this study, ranged between about 0.1 and more than 100 $\text{nmol m}^{-2} \text{s}^{-1}$, and averaged 8 $\text{nmol m}^{-2} \text{s}^{-1}$. This agrees reasonably well with Das et al. (2003) for maize (vertical gradient technique, $29 \pm 12 \text{ nmol m}^{-2} \text{s}^{-1}$). It is however much larger than those reported by Havermann et al. (2022) for rapeseed (chambers, average $2.5 \text{ nmol m}^{-2} \text{s}^{-1}$), and by Loubet et al. (2022) for winter wheat (EC, 0 to 4 $\text{nmol m}^{-2} \text{s}^{-1}$), as well as by Bachy et al. (2016, 2018, 2020) for maize and wheat (EC, 2.1 to 3 $\text{nmol m}^{-2} \text{s}^{-1}$). However, these fluxes were about five times smaller than those reported by Gonzaga Gomez et al. (2019) during the same experimental campaign (plant chambers, average flux of 37 to 39 $\text{nmol m}^{-2} \text{s}^{-1}$, considering a measured plant biomass of 780 g (dry matter) m^{-2} at maturity). Such a difference is explained by the higher temperature in the chambers leading to larger emissions. As suggested by the authors, scaling to the soil temperature would lead to a closer much agreement between eddy-covariance and chamber measurements (see *Appendix K* in Gonzaga Gomez et al. (2019)).

4.2 Exchange of other oxygenated BVOC

This study reported significant emission fluxes of two other oxygenated BVOC than methanol during the whole field campaign, namely acetaldehyde and acetone, which were also reported in other studies performed in rapeseed crops using continuous flux measurements with dynamic chambers (Gonzaga Gomez et al., 2019; Havermann et al., 2022). Voyard et al. (2024) also reported acetaldehyde emissions as one of the most emitted compounds from a rapeseed plant after methanol, in a chamber experiment. The emission of acetaldehyde during the senescence period, therefore in the presence of leaf litter, twice larger than during the fruit development period in this study, corroborates the chamber observations from Abis et al. (2021) that rapeseed leaf litter are a significant source. According to Seco et al. (2007), acetaldehyde emissions may result from various mechanisms, among which reactions to physical stress (cutting and drying of harvested crop material, which could be assimilated to drying leaf litter).

At the ecosystem scale, emission fluxes of acetaldehyde and acetone were reported on other crop species than rapeseed. In maize, Das et al. (2003) and Graus et al. (2013) reported acetone as the second most importantly emitted oxygenated BVOC, like in this study. Still in a maize field, Bachy et al. (2016) reported bidirectional fluxes of acetone and acetaldehyde, with emission during early crop development and then progressive reduction (even deposition) as the crop reaches late stages, which they attributed to a reduction in the soil source contribution. In a winter wheat crop, Bachy et al. (2020) also observed bidirectional fluxes of acetone and acetaldehyde, with



590 deposition during plant development stages and emission during senescence for both compounds, which tends to confirm the observations of the present study showing increased senescence-induced emission of methanol, acetone and acetaldehyde.

In this study, two oxygenated compounds had bidirectional behaviours: formaldehyde which was deposited in the fruit development stage and then emitted during senescence, and acetic acid, for which the opposite behaviour was observed. While bearing in mind the uncertainty in formaldehyde quantification, the fluxes observed in the present study were significant and showed a clear daily pattern (e.g. Fig. 4 C1 and C2). The formaldehyde behaviour switching from deposition during fruit development period to emission during senescence is similar to what was observed by Loubet et al. (2022) in a winter wheat field. Deposition fluxes of formaldehyde were also observed by Brillì et al. (2016) during the whole eddy-covariance measurement campaign performed in a poplar plantation. On the contrary, formaldehyde emission was reported by Gonzaga Gomez et al. (2019) on plant chambers during late flowering/fruit development stage, while deposition was measured by eddy-covariance. The reasons for these differences could be due to soil deposition not included in plant chambers, or higher temperatures in these devices than in the surrounding field (Gonzaga Gomez et al., 2019). Observations regarding acetic acid will be discussed in section 4.4.

600 Other oxygenated BVOC like m/z 73.064 (possibly methyl-ethyl-ketone (MEK) or ethyl-vinyl-ether), 83.049 (methylfuran and GLV fragments), 87.042 (butanedione), 87.078 (butenol (MBO), butanone), 101.059 (pentanedione) were emitted at small but significant rates during both vegetation stages. MEK and GLV were also reported by Brillì et al. (2016) and Havermann et al. (2022) over maize and rapeseed.

4.3 Emission of terpenoids, and sulphur- or nitrogen-containing BVOC

Emissions of terpenoid compounds, including isoprene, monoterpenes, sesquiterpenes and their associated fragments, were observed in the present study. Butcher et al. (1994, 1995) and Jakobsen et al. (1994), performed measurements of BVOC composition of the floral fragrances with Tenax TA and GC on different rapeseed flowering stages but did not report fluxes quantified at the plant level. Butcher et al. (1994, 1995) reported that terpenoids represented 59 to 74 % of the summed GC peaks, while Jakobsen et al. (1994), reported that sesquiterpenes and monoterpenes represented up to 90 % of the total measured floral BVOC flux of $45 \text{ ng flower}^{-1} \text{ hour}^{-1}$, a unit difficult to compare to the emitted amounts observed in other studies. These first studies did not measure all compounds and notably methanol, and focussed on flowers, which explains the high share of terpenoids they found compared to our study. More recently, Havermann et al. (2022) reported that monoterpenes, sesquiterpenes and oxygenated monoterpenes contributed to about 1 % in moles to total emitted BVOC, an amount comparable to our study.

620 A few emitted compounds detected by the PTR-Qi-TOF-MS were identified as BVOC possibly containing sulphur or nitrogen atoms. These were methanethiol (m/z 49.014), nitromethane (m/z 62.029), methyl vinyl sulphide (m/z 75.025), dimethyl sulfone (m/z 95.015), indole (m/z 118.074) and p-thiocresol (m/z 167.052). Among these compounds, methanethiol and dimethyl sulfone were recently reported by Voyard et al. (2024) as being emitted by soils, and methanethiol also emitted by rapeseed leaves and roots. Veromann et al. (2013) observed small emissions of indole by parasited rapeseed plants at various nitrogen crop fertilization rates.

625 4.4 Deposition of BVOC

Much fewer BVOC were deposited in the present study than those observed in winter wheat fields (Bachy et al., 2020; Loubet et al., 2022). Indeed, out of the BVOC seen to be deposited in Loubet et al. (2022), only formic acid



and acetic acid exhibited similar behaviour in the present study, the latter showing bi-directional fluxes. Deposition
fluxes of acetic acid were reported by Bachy et al. (2020) over a winter wheat crop, from emergence to senescence,
630 and by Bachy et al. (2016) over bare soil. In the present study, acetic acid was depositing during the senescence
stage, but showed small (down to $-0.05 \text{ nmol m}^{-2} \text{ s}^{-1}$) nocturnal deposition fluxes and large daily emissions (up to
 $0.2 \text{ nmol m}^{-2} \text{ s}^{-1}$) during fruit development period. Kesselmeier et al. (1998) showed that uptake of acetic and
formic acids in crop plants were related to the stomatal opening for crops like corn, pea and barley (rapeseed was
not investigated), which is not fully consistent with the present study as during senescence, plant cells are less and
635 less active. Acetic acid uptake by the soil could therefore constitute a more likely explanation, as suggested by
Bachy et al. (2016, 2020). Gomez et al. (2021), found that acetic acid switched from deposition to emission fluxes
when the plant entered senescence, which is opposite to what was observed in the present study at the ecosystem
level, suggesting that when the plant parts get degraded, acetic acid may be released from the plant but would then
be deposited on the soil or elsewhere within the whole crop canopy.

640 Differences with observations by Loubet et al. (2022) also relate to methylfuran and GLV fragments (m/z 83.049)
and pentanedione (m/z 101.059), which were emitted in the present study but deposited in their study over a winter
wheat field. Besides, ion m/z 43.018 did not show a significant flux over rapeseed, contrary to Loubet et al. (2022),
who found a significant deposition flux. Also, while deposition fluxes of methanol at night were observed in winter
wheat fields (Bachy et al., 2020; Loubet et al., 2022), this was not the case in the present work. The observation
645 of few deposited compounds and small deposition fluxes compared to Loubet et al. (2022) could be explained by
the closed-canopy structure of rapeseed compared to winter wheat, which would prevent methanol and other
soluble BVOC from being absorbed by the soil.

4.6 BVOC flux diel patterns

All BVOC in this study exhibited diel emission or deposition patterns (Fig. 4 and S04). The peak emission times
650 occurred between mid-day and early afternoon for most compounds, confirming the roles played by radiation
and/or temperature in driving BVOC emissions, as it was also observed in previous works (e. g. Guenther et al.,
1995). However, differences between BVOC in the timing of emission increase at the beginning of the day were
observed. Methanol (in both sub-periods) and methanethiol (in sub-period 2) exhibited emission increases starting
as of 6 am UTC, as radiation also started to increase (Fig. 4 E1 and E2). The coincidence of the flux increase with
655 solar radiation suggests a stomatal pathway for these compounds. The emission burst would be explained by the
release from plant water where these compounds may have accumulated overnight through metabolic processes.
Emission bursts of methanol in relation to stomata closure/aperture have been reported in previous studies (e.g.
Harley et al., 2007; Hüve et al., 2007; Mozaffar et al., 2017). However, while emission bursts in the morning were
also reported for other BVOC like acetaldehyde and acetone in a poplar forest equipped with cuvettes (Brilli et al.,
660 2014a), this was observed for these compounds in the present study.

4.7 Effect of senescence on BVOC emissions

The absolute magnitude of the fluxes of oxygenated compounds like methanol, acetone, acetaldehyde,
formaldehyde, formic acid, acetic acid increased during the senescence period. This can be related to both
environmental and plant physiological characteristics. All these oxygenated soluble compounds make them more
665 storable in foliar water pools (Niinemets et al., 2004), which makes them prone to be released during senescence
when the stomatal control becomes less efficient. Increased methanol and acetone emissions during senescence
have been recently reported for wheat and maize (Bachy et al., 2018, 2020; Gomez et al., 2021; Gonzaga Gomez
et al., 2019; Mozaffar et al., 2017, 2018), but to our knowledge, there is no information in the literature for



670 rapeseed, as Havermann et al. (2022) investigated inflorescence emergence and flowering for this crop, but not senescence stages. In the case of methanol and acetone, larger emissions during senescence could also result from the breakdown of cellular structures from both above-ground and below-ground plant parts (Mozaffar et al., 2018; Rottenberger et al., 2005; Voyard et al., 2024), a process analogous to those occurring during plant growth and cell wall expansion (Fall and Benson, 1996). Increased emissions of acetaldehyde during late senescence were also reported in wheat by Bachy et al. (2020).

675 Emissions of terpenoid compounds remained in the same range or, opposite to oxygenated compounds behaviour, were seen to slightly decrease (e.g. sesquiterpenes, Fig. S04) during senescence. The decrease in monoterpenes emissions aligns with observations for rapeseed at the plant scale by Gomez et al. (2021), who also observed a decrease in monoterpenes emissions as the plant entered senescence. Conversely, in the study by Bachy et al. (2020) on winter wheat, isoprene and monoterpenes emissions increased slightly during the senescence period.

680 **4.8 BVOC standard emission factors (SEF) and implication for OH reactivity**

SEF (standard emission factor) estimates for crops are scarce in the literature. In the MEGAN2.1 model, the BVOC (biogenic volatile organic compound) emission profile is assumed to be nearly identical across all crop species, with the exception that some crops do not emit isoprene. Moreover, MEGAN2.1 does not differentiate between crop developmental stages (Guenther et al., 1995; Karl et al., 2009).

685 In this study, SEFs were determined for rapeseed during both the fruit development and senescence stages (Table 2). Methanol SEFs were about 30% larger during senescence compared to fruit development, but they were about 30 % to 50 % smaller than the values used in MEGAN2.1 (Guenther et al., 2012) and three to four times higher than those reported by Havermann et al. (2022). For terpenoids, isoprene and monoterpene SEFs were 2 to 13 times higher than in MEGAN2.1, while isoprene SEFs were on average in the same range as those reported by
690 Gonzaga Gomez et al. (2019). Sesquiterpenes SEFs were comparable to MEGAN2.1 estimates.

Our findings suggest that the contributions of methanol and acetaldehyde to OH reactivity may be overestimated by MEGAN2.1 while those of isoprene and monoterpenes, would be underestimated by this model during active plant development, and to a lesser extent during senescence. While flowering was not investigated, this study highlights the importance of accounting for crop development stages when evaluating BVOC emissions. In
695 MEGAN2.1, OH reactivity is mainly attributed to green leaf volatiles and stress-related BVOCs such as indole. However, indole SEFs are about 300 times higher in MEGAN2.1 than in our study (Table 2). Guenther et al. (2012) acknowledged the uncertainties in SEFs for such compounds, due to both limited measurements and their sensitivity to plant damage. Our results indicate that these emissions are likely minimal during late stages of oilseed rape. The OH reactivity constant of indole used here was taken from Atkinson et al. (1995) and confirmed by Xue
700 et al. (2022), supporting the robustness of our calculations. Methanethiol and 4-oxopentanal SEFs were also found to be 50–60 times higher in MEGAN2.1 than in this study (Table 2). In MEGAN2.1, these compounds significantly contribute to OH reactivity, while our data suggest they are minor sources. They are thought to originate from leaf surface waxes exposed to ozone and UV (Fruekilde et al., 1998).

Although methanol contributed substantially to total BVOC emissions from rapeseed, its role in OH reactivity was
705 limited (about 18%), consistent with Bsaibes et al. (2020). The larger contribution (about 30 %) to total OH reactivity by formaldehyde was similarly observed through this study and MEGAN2.1 estimates. However, as mentioned earlier in this study, there exists uncertainties in formaldehyde quantification, which tend to prevent robust conclusions to be drawn for this compound. Instead, rapeseed was found to be a stronger source of



710 terpenoids than previously assumed in MEGAN2.1. Because terpenoids have OH reaction constants about 100
times higher than methanol (Atkinson and Arey, 2003), they dominated OH reactivity, accounting for 44 % of the
total. This is in the same range as the 40 % isoprenoid contribution reported by Bsaibes et al. (2020) in the same
field experiment, who based their estimates on concentrations rather than emissions. These figures are more than
five times larger than what is assumed in MEGAN2.1 for these compounds. This suggests that MEGAN2.1
underestimates the role of terpenoids and isoprenoids. This underestimation could have implications for secondary
715 organic aerosol (SOA) formation, as terpenoids and isoprenoids (isoprene, monoterpenes, sesquiterpenes) are far
more effective SOA precursors than methanol, acetone, or acetaldehyde (Sakulyanontvittaya et al., 2008).

4.9 Hypothesis to explain the observed uncommon large deposition fluxes of isoprenoids and siloxanes

We found overall good agreement in both magnitude and temporal dynamics between the mixing ratios measured
with the EC and profile setups at the same sampling height of 3.0 m (Fig. S05a–d) for most compounds. Moreover,
720 isoprene mixing ratios were consistent in both dynamics and magnitude compared to those from a permanent air
quality station in Paris (V. Gros, pers. comm.). These good agreements strengthen confidence in the accuracy of
BVOC quantification during the campaign, and in turn in the observed high deposition fluxes during sub-periods
3 and 4 for compounds typically considered as emitted species (Fig. 6).

The hypothesis of a regional pollution event from Paris seems unlikely, given the high reactivity of the compounds
725 involved (e.g., monoterpenes, isoprene; Table 2). A more plausible explanation is the local advection of a plume
enriched in siloxanes and terpenes (Fig. 7). Such a plume would also contain other highly reactive species, to
explain the strong chemical sinks of these compounds observed in the profile tubes. To explore this possibility,
we gathered information on agricultural operations (e.g., pesticide applications, fertilizer use) in adjacent fields,
and found that maize was planted in a nearby field located north-east of the site during the campaign. This suggests
730 that herbicides may have been applied, as this is a common practice in the region. Herbicide formulations contain
adjuvants and solvents, sometimes including organo-silicone compounds such as siloxanes (e.g. Li et al., 2019;
Chen et al., 2022) like the commercial product Silwet® (EPHY, 2025) which we know was occasionally applied
at the farm scale (e.g., Silwet). In addition, herbicide application damages or destroys plants, which can trigger
large pulses of terpenoid emissions, similar to those observed after herbivory (Piesik et al., 2011; Kammer et al.,
735 2019) or extreme meteorological events (Bamberger et al., 2011). Based on this evidence, we hypothesise that
herbicide application in adjacent fields may have generated a plume containing siloxanes and terpenes, leading to
the observed concentration peaks and deposition fluxes at our site. While plausible, this explanation remains
speculative and would require further targeted experiments to be confirmed.

5 Conclusion

740 To our knowledge, this study is the first one to report BVOC fluxes measured by the eddy-covariance technique
from a rapeseed field. This technique allowed us to quantify BVOC fluxes continuously at the field scale without
disturbing the ecosystem. It showed that oxygenated BVOC, and above all, methanol, are the main BVOC emitted
by this crop type. Notably, methanol contributed more than 90 % to the summed molar-based emissions during
vegetated and bare soil periods. As part of 42 compounds with significant fluxes, the other major emitted
745 compounds were acetone, monoterpenes, isoprene, formaldehyde and methanethiol. Few compounds were seen to
be deposited during both fruit development and senescence periods, among which formic and acetic acids were
the most deposited ones. BVOC diel emission patterns were related to air temperature and solar radiation
dynamics.



750 Uncommonly large deposition fluxes of certain BVOC (among which monoterpenes, isoprene, and siloxanes) were observed over two specific and short periods in May. Wind direction, reactivity analysis, and local management suggest local advection of these compounds from agricultural activity in the neighbouring fields may be the cause of this atypical deposition observation. Our results further suggest that the use of two lines with differing time responses at the same height (EC and profiles) mixing ratio could be useful to investigate BVOC atmospheric reactivity in the field.

755 The standard emission factors (SEF) computed in this study are based on a non-invasive method (eddy-covariance) and representative of the whole ecosystem. The methanol SEF calculated in the present study were about 30 % smaller than those proposed in the model MEGAN2.1 for crops, while terpenoid SEF were larger by a factor between 2 and 13 compared to crops SEF in MEGAN2.1. These new emission factors would substantially modify the contribution of rapeseed to atmospheric OH reactivity, for which the contribution of terpenoids would be more
760 critical than previously reported, therefore playing a significant role in SOA formation.

Author contribution

All co-authors contributed to this field campaign of the COV3ER project. PB analysed the data, initiated and wrote the manuscript with contributions of all co-authors, BL, RC, FL, CD and VG designed the field experiment. BD, OZ, JCG and OF carried out most of the technical work during the experiment, LGG performed BVOC chamber
765 measurements during the field campaign, SB performed OH reactivity measurements during the field campaign, NZ thoroughly reviewed the manuscript.

Competing interests

The authors declare that they have no conflict of interest.

Data Availability

770 Meteorological and BVOC flux datasets, as well as scripts can be found at <https://doi.org/10.57745/AIINCW> .

ICOS data are accessible at the ICOS carbon portal:

Buysse, P., Loubet, B., Depuydt, J., Durand, B., Gueudet, J. (2024). Fluxnet Archive Product from Grignon, 2004–2023, FLUXNET, https://hdl.handle.net/11676/78Q_tkc0nWxtTDAo1Of0UHoB

Acknowledgements

775 This study was supported by the region Île-de-France (DIM R2DS, Réseau francilien de Recherche sur le Développement Soutenable, project n° 1656), ADEME (COV3ER, project n°1562C0032) and the EU ICOS Research Infrastructure consortium. The PTR-Qi-ToF-MS is a national instrument supported by ANAEE-FR services (ANR project n°11-INBS-0001). We gratefully thank the AgroParisTech farm, for giving us access to their fields, and Dominique Tristant for providing detailed information on the crop management.



780 **References**

- Abis, L., Kalalian, C., Lunardelli, B., Wang, T., Zhang, L., Chen, J., Perrier, S., Loubet, B., Ciuraru, R., and George, C.: Measurement report: Biogenic volatile organic compound emission profiles of rapeseed leaf litter and its secondary organic aerosol formation potential, *Atmospheric Chemistry and Physics*, 21, 12613–12629, <https://doi.org/10.5194/acp-21-12613-2021>, 2021.
- 785 Acton, W.J.F., Schallhart, S., Langford, B., Valach, A., Tantala, P., Fares, S., Carriero, G., Tillmann, R., Tomlinson, S.J., Dragosits, U., Gianelle, D., Hewitt, C.N., and Nemitz, E.: Canopy-scale flux measurements and bottom-up emission estimates of volatile organic compounds from a mixed oak and hornbeam forest in northern Italy, *Atmos. Chem. Phys.*, 16, 7149–7170, doi:10.5194/acp-16-7149-2016, 2016.
- 790 Acton, W.J.F., Huang, Z., Davison, B., Drysdale, W.S., Fu, P., Hollaway, M., Langford, B., Lee, J., Liu, Y., Metzger, S., Mullinger, N., Nemitz, E., Reeves, C.E., Squires, F.A., Vaughan, A.R., Wang, X., Wang, Z., Wild, O., Zhang, Q., Zhang, Y., and Hewitt, C.N.: Surface-atmosphere fluxes of volatile organic compounds in Beijing 2020, *Atmos. Chem. Phys.*, 20, 15101–15125, <https://doi.org/10.5194/acp-20-15101-2020>, 2020.
- 795 AHDB, 2023, <https://ahdb.org.uk/knowledge-library/the-growth-stages-of-oilseed-rape> last consulted on 07/07/2023
- Atkinson, R., Tuazon, E.C., Arey, J., and Aschmann, S.M.: Atmospheric and indoor chemistry of gas-phase indole, quinoline, and isoquinoline, *Atmospheric Environment*, 29(23), 3423–3432, 1995.
- Atkinson, R. and Arey, J.: Gas-phase tropospheric chemistry of biogenic volatile organic compounds: a review, *Atmospheric Environment*, 37, 197–219, [https://doi.org/10.1016/S1352-2310\(03\)00391-1](https://doi.org/10.1016/S1352-2310(03)00391-1), 2003.
- 800 Aubinet, M., Grelle, A., Ibrom, A., Rannik, U., Moncrieff, J., Foken, T., Kowalski, A. S., Martin, P. H., Berbigier, P., Bernhofer, C., Clement, R., Elbers, J., Granier, A., Grunwald, T., Morgenstern, K., Pilegaard, K., Rebmann, C., Snijders, W., Valentini, R., and Vesala, T.: Estimates of the annual net carbon and water exchange of forests: The EUROFLUX methodology, *Adv. Ecol. Res.*, 30, 113–175, 2000.
- 805 Bachy, A., Aubinet, M., Schoon, N., Amelynck, C., Bodson, B., Moureaux, C., and Heinesch, B.: Are BVOC exchanges in agricultural ecosystems overestimated? Insights from fluxes measured in a maize field over a whole growing season, *Atmos. Chem. Phys.*, 16, 5343–5356, <https://doi.org/10.5194/acp-16-5343-2016>, 2016.
- 810 Bachy, A., Aubinet, M., Amelynck, C., Schoon, N., Bodson, B., Moureaux, C., Delaplace, P., De Ligne, A., and Heinesch, B.: Methanol exchange dynamics between a temperate cropland soil and the atmosphere, *Atmospheric Environment*, 176, 229–239, <https://doi.org/10.1016/j.atmosenv.2017.12.016>, 2018.
- Bachy, A., Aubinet, M., Amelynck, C., Schoon, N., Bodson, B., Delaplace, P., De Ligne, A., Digrado, A., du Jardin, P., Fauconnier, M.-L., Mozaffar, A., Müller, J.-F., and Heinesch, B.: Dynamics and mechanisms of volatile organic compound exchanges in a winter wheat field, *Atmospheric Environment*, 221, 117105, <https://doi.org/10.1016/j.atmosenv.2019.117105>, 2020.
- 815 Bamberger, I., Hörtnagl, L., Ruuskanen, T.M., Schnitzhofer, R., Müller, M., Graus, M., Karl, T., Wohlfahrt, G., and Hansel, A.: Deposition fluxes of terpenes over grassland, *Journal of Geophysical Research*, Vol. 116, D14305, doi:10.1029/2010JD015457, 2011.
- 820 Boy, M., Kurtén, T., Chen, D., Xavier, C., Clusius, P., Roldin, P., Baykara, M., Pichelstorfer, L., Foreback, B., Bäck, J., Petäjä, T., Makkonen, R., Kerminen, V.-M., Pihlatie, M., Aalto, J., and Kulmala, M.: Positive feedback mechanism between biogenic volatile organic compounds and the methane lifetime in future climates, *Climate and Atmospheric Science* 5:72, <https://doi.org/10.1038/s41612-022-00292-0>, 2022.
- 825 Brilli, F., Gioli, B., Zona, D., Pallozzi, E., Zenone, T., Fratini, G., Calfapietra, C., Loreto, F., Janssens, I. A., and Ceulemans, R.: Simultaneous leaf- and ecosystem-level fluxes of volatile organic compounds from a poplar-based SRC plantation, *Agricultural and Forest Meteorology*, 187, 22–35, <https://doi.org/10.1016/j.agrformet.2013.11.006>, 2014a.
- Brilli, F., Gioli, B., Ciccioli, P., Zona, D., Loreto, F., Janssens, I.A., Ceulemans, R.: Proton Transfer Reaction Time-of-Flight Mass Spectrometric (PTR-TOFMS) determination of volatile organic compounds (VOCs) emitted from a biomass fire developed under stable nocturnal conditions, *Atmospheric Environment*, 97, 54–67, 2014b
- 830 Brilli, F., Gioli, B., Fares, S., Terenzio, Z., Zona, D., Gielen, B., Loreto, F., Janssens, I. A., and Ceulemans, R.: Rapid leaf development drives the seasonal pattern of volatile organic compound (VOC) fluxes in a ‘coppiced’ bioenergy poplar plantation: Seasonality of VOC fluxes in coppiced poplars, *Plant, Cell & Environment*, 39, 539–555, <https://doi.org/10.1111/pce.12638>, 2016.
- 835 Bsaiibes, S., Gros, V., Truong, F., Boissard, C., Baisnée, D., Sarda-Esteve, R., Zannoni, N., Lafouge, F., Ciuraru, R., Buysse, P., Kammer, J., Gomez, L. G., and Loubet, B.: Characterization of Total OH Reactivity in a Rapeseed Field: Results from the COV3ER Experiment in April 2017, *Atmosphere*, 11, 261, <https://doi.org/10.3390/atmos11030261>, 2020.
- 840 Butcher, R. D., Macfarlane-Smith, W., Robertson, G. W., and Griffiths, D. W.: The identification of potential aeroallergen/irritant(s) from oilseed rape (*Brassica napus* spp. *oleifera*): volatile organic compounds



- emitted during flowering progression, *Clinical & Experimental Allergy*, 24, 1105–1114, <https://doi.org/10.1111/j.1365-2222.1994.tb03315.x>, 1994.
- 845 Butcher, R. D., Goodman, B. A., and Deighton, N.: Evaluation of the allergic/irritant potential of air pollutants: detection of proteins modified by volatile organic compounds from oilseed rape (*Brassica napus* ssp. *oleiferd*) using electrospray ionization-mass spectrometry, *Clin Exp Allergy*, 25, 985–992, <https://doi.org/10.1111/j.1365-2222.1995.tb00401.x>, 1995.
- Chen, S., Xu, Z., Liu, P., Zhuang, Y., Jiang, M., Zhang, X., Han, Z., Liu, Y., Chen, X.: Assessment of volatile organic compound emissions from pesticides in China and their contribution to ozone formation potential, *Environ. Monit. Assess.*, 194:737, <https://doi.org/10.1007/s10661-022-10423-y>, 2022.
- 850 Courtois, E. A., Paine, C. E. T., Blandinieres, P.-A., Stien, D., Bessiere, J.-M., Houel, E., Baraloto, C., and Chave, J.: Diversity of the Volatile Organic Compounds Emitted by 55 Species of Tropical Trees: a Survey in French Guiana, *J Chem Ecol*, 35, 1349–1362, <https://doi.org/10.1007/s10886-009-9718-1>, 2009.
- 855 Das, M., Kang, D., Aneja, V. P., Lonneman, W., Cook, D. R., and Wesely, M. L.: Measurements of hydrocarbon air–surface exchange rates over maize, *Atmospheric Environment*, 37, 2269–2277, [https://doi.org/10.1016/S1352-2310\(03\)00076-1](https://doi.org/10.1016/S1352-2310(03)00076-1), 2003.
- Ephy, 2025, <https://ephy.anses.fr/adjuvant/silwet-77>, last consulted 16/04/2025
- Fall, R., and Benson, A.A.: Leaf methanol — the simplest natural product from plants. *Trends Plant Sci.* 1, 296–301. [https://doi.org/10.1016/S1360-1385\(96\)88175-0](https://doi.org/10.1016/S1360-1385(96)88175-0), 1996.
- 860 FAOSTAT 2023, <https://www.fao.org/faostat/en/#home>, last consulted 07/07/2023
- Flechar, C. R., Massad, R. S., Loubet, B., Personne, E., Simpson, D., Bash, J. O., Cooter, E. J., Nemitz, E., and Sutton, M. A.: Advances in understanding, models and parameterizations of biosphere-atmosphere ammonia exchange, *Biogeosciences*, 10, 5183–5225, 10.5194/bg-10-5183-2013, 2013.
- 865 Fruekilde, P., Hjorth, J., Jensen, N. R., Kotzias, D., and Larsen, B.: Ozonolysis at vegetation surfaces: A source of acetone, 4-oxopentanal, 6-methyl-5-hepten-2-one, and geranyl acetone in the troposphere, *Atmospheric Environment*, 32(11), 1893–1902, 1998.
- Gallagher, M. W., Clayborough, R., Beswick, K. M., Hewitt, C. N., Owen, S., Moncrie, J., and Pilegaard, K.: Assessment of a relaxed eddy accumulation for measurements of fluxes of biogenic volatile organic compounds: study over arable crops and a mature beech forest, *Atmospheric Environment*, 13, 2000.
- 870 Gomez, L. G., Loubet, B., Lafouge, F., Ciuraru, R., Bsaibes, S., Kammer, J., Buysse, P., Durand, B., Gueudet, J.-C., Fanucci, O., Zurfluh, O., Decuq, C., Truong, F., Gros, V., and Boissard, C.: Effect of senescence on biogenic volatile organic compound fluxes in wheat plants, *Atmospheric Environment*, 266, 118665, <https://doi.org/10.1016/j.atmosenv.2021.118665>, 2021.
- 875 Gonzaga Gomez, L., Loubet, B., Lafouge, F., Ciuraru, R., Buysse, P., Durand, B., Gueudet, J.-C., Fanucci, O., Fortineau, A., Zurfluh, O., Decuq, C., Kammer, J., Duprix, P., Bsaibes, S., Truong, F., Gros, V., and Boissard, C.: Comparative study of biogenic volatile organic compounds fluxes by wheat, maize and rapeseed with dynamic chambers over a short period in northern France, *Atmospheric Environment*, 214, 116855, <https://doi.org/10.1016/j.atmosenv.2019.116855>, 2019.
- 880 Graus, M., Eller, A. S. D., Fall, R., Yuan, B., Qian, Y., Westra, P., de Gouw, J., and Warneke, C.: Biosphere-atmosphere exchange of volatile organic compounds over C4 biofuel crops, *Atmospheric Environment*, 66, 161–168, <https://doi.org/10.1016/j.atmosenv.2011.12.042>, 2013.
- Gros, V., and Zannoni, N.: Total OH Reactivity. In: Dulac, F., Sauvage, S., Hamonou, E. (eds) *Atmospheric Chemistry in the Mediterranean Region*. Springer, Cham., https://doi.org/10.1007/978-3-030-82385-6_7, 2022.
- 885 Guenther, A.: Seasonal and spatial variations in natural volatile organic compound emissions, *Ecological Applications*, 7, 34–45, [https://doi.org/10.1890/1051-0761\(1997\)007\[0034:SASVIN\]2.0.CO;2](https://doi.org/10.1890/1051-0761(1997)007[0034:SASVIN]2.0.CO;2), 1997.
- Guenther, A., Hewitt, C. N., Erickson, D., Fall, R., Geron, C., Graedel, T., Harley, P., Klinger, L., Lerdau, M., Mckay, W. A., Pierce, T., Scholes, B., Steinbrecher, R., Tallamraju, R., Taylor, J., and Zimmerman, P.: A global model of natural volatile organic compound emissions, *J. Geophys. Res.*, 100, 8873, <https://doi.org/10.1029/94JD02950>, 1995.
- 890 Guenther, A. B., Jiang, X., Heald, C. L., Sakulyanontvittaya, T., Duhl, T., Emmons, L. K., and Wang, X.: The Model of Emissions of Gases and Aerosols from Nature version 2.1 (MEGAN2.1): an extended and updated framework for modeling biogenic emissions, *Geosci. Model Dev.*, 5, 1471–1492, <https://doi.org/10.5194/gmd-5-1471-2012>, 2012.
- 895 Harley, P., Greenberg, J., Niinemets, U., and Guenther, A.: Environmental controls over methanol emission from leaves, *Biogeosciences*, 4, 1083–1099, 2007.
- Havermann, F., Ghirardo, A., Schnitzler, J., Nendel, C., Hoffmann, M., Kraus, D., and Grote, R.: Modeling Intra- and Interannual Variability of BVOC Emissions From Maize, Oil-Seed Rape, and Ryegrass, *J. Adv. Model. Earth Syst.*, 14, <https://doi.org/10.1029/2021MS002683>, 2022.
- 900 Holzinger, R., Acton, W.J.F., Bloss, W.J., Breitenlechner, M., Crilley, L.R., Dusanter, S., Gonin, M., Gros, V., Keutsch, F.N., Kiendler-Scharr, A., Kramer, L.J., Krechmer, J.E., Languille, B., Locoge, N., Lopez-Hilfiker, F., Materić, D., Moreno, S., Nemitz, E., Quéléver, L.L.J., Sarda Esteve, R., Sauvage, S., Schallhart, S., Sommariva, R., Tillmann, R., Wedel, S., Worton, D.R., Xu, K. and Zaytsev A.: Validity and limitations of simple reaction kinetics to calculate concentrations of organic compounds from ion



- 905 counts in PTR-MS, *Atmospheric Measurement Techniques* 12, 6193–6208, <https://doi.org/10.5194/amt-12-6193-2019>, 2019.
- Hüve, K., Christ, M., Kleist, E., Uerlings, R., Niinemets, Ü., Walter, A., and Wildt, J.: Simultaneous growth and emission measurements demonstrate an interactive control of methanol release by leaf expansion and stomata, *Journal of Experimental Botany*, 58, 1783–1793, <https://doi.org/10.1093/jxb/erm038>, 2007.
- 910 Isaksen, I. S. A., Granier, C., Myhre, G., Berntsen, T. K., Dalsøren, S. B., Gauss, M., Klimont, Z., Benestad, R., Bousquet, P., Collins, W., Cox, T., Eyring, V., Fowler, D., Fuzzi, S., Jöckel, P., Laj, P., Lohmann, U., Maione, M., Monks, P., Prevo, A. S. H., Raes, F., Richter, A., Rognerud, B., Schulz, M., Shindell, D., Stevenson, D. S., Storelvmo, T., Wang, W.-C., van Weele, M., Wild, M., and Wuebbles, D.: Atmospheric composition change: Climate–Chemistry interactions, *Atmospheric Environment*, 43, 5138–5192, <https://doi.org/10.1016/j.atmosenv.2009.08.003>, 2009.
- 915 IUPAC, 2023, IUPAC Task Group on Atmospheric Chemical Kinetic Data Evaluation – Data Sheet HO_x_VOCl1 (ipsl.fr)
- Jakobsen, H.B., Friis, P., Nielsen, J.K., and Olsen, C.E.: Emission of volatiles from flowers and leaves of *Brassica napus* in situ, *Phytochemistry*, 37(3), 695–699, 1994.
- 920 Jensen, N.R., Gruening, C., Goded, I., Müller, M., Hjorth, J., and Wisthaler, A.: Eddy-covariance flux measurements in an Italian deciduous forest using PTR-ToF-MS, PTR-QMS and FIS, *International Journal of Environmental Analytical Chemistry*, 98:8, 758–788, DOI: 10.1080/03067319.2018.1502758, 2018.
- Jiao, Y., Acdan, J., Xu, R., Deventer, M.J., Zhang, W., and Rhew, R.C.: Global Methyl Halide Emissions From Rapeseed (*Brassica napus*) Using Life Cycle Measurements, *Geophysical Research Letters*, 47, e2020GL089373, <https://doi.org/10.1029/2020GL089373>, 2020.
- Kammer, J., Lafouge, F., Décuq, C., Ciuraru, R., Bedos, C., Baisnée, D., Bonnaire, N., Sbaibes, S., Buysse, P., Durand, B., Petit, J.-E., Sarda-Estève, R., Truong, F., Gros, V., Loubet, B.: Effect of agricultural practices on volatile organic compound (VOC) emissions from winter wheat. 8th International PTR-MS Conference 2019, Feb 2019, Innsbruck, Austria. (hal-02786054)
- 930 Kammer, J., Décuq, C., Baisnée, D., Ciuraru, R., Lafouge, F., Buysse, P., Sbaibes, S., Henderson, B., Cristescu, S. M., Benabdallah, R., Chandra, V., Durand, B., Fanucci, O., Petit, J.-E., Truong, F., Bonnaire, N., Sarda-Estève, R., Gros, V., and Loubet, B.: Characterization of particulate and gaseous pollutants from a French dairy and sheep farm, *Science of The Total Environment*, 712, 135598, <https://doi.org/10.1016/j.scitotenv.2019.135598>, 2020.
- 935 Kaplan, J. O., Folberth, G., and Hauglustaine, D. A.: Role of methane and biogenic volatile organic compound sources in late glacial and Holocene fluctuations of atmospheric methane concentrations, *Global Biogeochem. Cycles*, 20, <https://doi.org/10.1029/2005GB002590>, 2006.
- Karl, T., Guenther, A., Lindinger, C., Jordan, A., Fall, R., and Lindinger, W.: Eddy covariance measurements of oxygenated volatile organic compound fluxes from crop harvesting using a redesigned proton-transfer-reaction mass spectrometer, *J. Geophys. Res.*, 106, 24157–24167, <https://doi.org/10.1029/2000JD000112>, 2001.
- 940 Karl, M., Guenther, A., Koble, R., Leip, A., and Seufert, G.: A new European plant-specific emission inventory of biogenic volatile organic compounds for use in atmospheric transport models, *Biogeosciences*, 6, 1059–1087, 2009.
- 945 Kesselmeier, J., Bode, K., Gerlach, C., and Jork, E.-M.: Exchange of atmospheric formic and acetic acids with trees and crop plants under controlled chamber and purified air conditions, *Atmospheric Environment*, 32, 1765–1775, [https://doi.org/10.1016/S1352-2310\(97\)00465-2](https://doi.org/10.1016/S1352-2310(97)00465-2), 1998.
- Kljun, N., Calanca, P., Rotach, M. W., and Schmid, H. P.: A simple two-dimensional parameterisation for Flux Footprint Prediction (FFP), *Geosci. Model Dev.*, 8, 3695–3713, doi:10.5194/gmd-8-3695-2015, 2015.
- 950 Konig, G.: Relative contribution of oxygenated hydrocarbons to the total biogenic VOC emissions of selected mid-European agricultural and natural plant species, *Atmospheric Environment*, 29, 861–874, [https://doi.org/10.1016/1352-2310\(95\)00026-U](https://doi.org/10.1016/1352-2310(95)00026-U), 1995.
- Koss, A. R., Sekimoto, K., Gilman, J. B., Selimovic, V., Coggon, M. M., Zarzana, K. J., Yuan, B., Lerner, B. M., Brown, S. S., Jimenez, J. L., Krechmer, J., Roberts, J. M., Warneke, C., Yokelson, R. J., and de Gouw, J.: Non-methane organic gas emissions from biomass burning: identification, quantification, and emission factors from PTR-ToF during the FIREX 2016 laboratory experiment, *Atmos. Chem. Phys.*, 18, 3299–3319, <https://doi.org/10.5194/acp-18-3299-2018>, 2018.
- 955 Langford, B., Acton, W., Ammann, C., Valach, A., and Nemitz, E.: Eddy-covariance data with low signal-to-noise ratio: time-lag determination, uncertainties and limit of detection, *Atmos. Meas. Tech.*, 8, 4197–4213, <https://doi.org/10.5194/amt-8-4197-2015>, 2015.
- 960 Li, B., Liu, Y., Zhang, P., Li, X., Pang, X., Zhao, Y., Li, H., Liu, F., Lin, J., Mu, W.: Selection of organosilicone surfactants for tank-mixed pesticides considering the balance between synergistic effects on pests and environmental risks, *Chemosphere*, 217, 591–598, <https://doi.org/10.1016/j.chemosphere.2018.11.061>, 2019.
- 965 Loubet, B., Laville, P., Lehuger, S., Larmanou, E., Fléchar, C., Mascher, N., Genermont, S., Roche, R., Ferrara, R. M., Stella, P., Personne, E., Durand, B., Decuq, C., Flura, D., Masson, S., Fanucci, O., Rampon, J.-N.,



- Siemens, J., Kindler, R., Gabrielle, B., Schrupf, M., and Cellier, P.: Carbon, nitrogen and Greenhouse gases budgets over a four years crop rotation in northern France, *Plant Soil*, 343, 109–137, <https://doi.org/10.1007/s11104-011-0751-9>, 2011.
- 970 Loubet, B., Buysse, P., Gonzaga-Gomez, L., Lafouge, F., Ciuraru, R., Decuq, C., Kammer, J., Bsaibes, S., Boissard, C., Durand, B., Guedet, J.-C., Fanucci, O., Zurfluh, O., Abis, L., Zannoni, N., Truong, F., Baisnée, D., Sarda-Estève, R., Staudt, M., and Gros, V.: Volatile organic compound fluxes over a winter wheat field by PTR-Qi-TOF-MS and eddy covariance, *Atmos. Chem. Phys.*, 22, 2817–2842, <https://doi.org/10.5194/acp-22-2817-2022>, 2022.
- 975 Mahilang, M., Deb, M. K., and Pervez, S.: Biogenic secondary organic aerosols: A review on formation mechanism, analytical challenges and environmental impacts, *Chemosphere*, 262, 127771, <https://doi.org/10.1016/j.chemosphere.2020.127771>, 2021.
- Manco, A., Brillio, F., Famulari, D., Gasbarra, D., Gioli, B., Vitale, L., Tommasi, P. di, Loubet, B., Arena, C., and Magliulo, V.: Cross-correlations of Biogenic Volatile Organic Compounds (BVOC) emissions typify different phenological stages and stressful events in a Mediterranean Sorghum plantation, *Agricultural and Forest Meteorology*, 303, 108380, <https://doi.org/10.1016/j.agrformet.2021.108380>, 2021.
- 980 McEwan, M. and Macfarlane Smith, W.H.: Identification of volatile organic compounds emitted in the field by oilseed rape (*Brassica napus* ssp. *oleifera*) over the growing season, *Clinical & Experimental Allergy*, 28, 332–338, <https://doi.org/10.1046/j.1365-2222.1998.00234.x>, 1998.
- 985 Millet, D.B., Alwe, H.D., Chen, X., Deventer, M.J., Griffis, T.J., Holzinger, R., Bertman, S.B., Rickly, B.S., Stevens, B.S., Léonardis, T., Locoge, N., Dusanter, S., Tyndall, G.S., Alvarez, S.L., Erickson, M.H., and Flynn, J.H.: Bidirectional Ecosystem–Atmosphere Fluxes of Volatile Organic Compounds Across the Mass Spectrum: How Many Matter?, *ACS Earth Space Chem.* 2, 8, 764–777, <https://doi.org/10.1021/acsearthspacechem.8b00061>, 2018.
- 990 Morrison, E. C., Drewer, J., and Heal, M. R.: A comparison of isoprene and monoterpene emission rates from the perennial bioenergy crops short-rotation coppice willow and *Miscanthus* and the annual arable crops wheat and oilseed rape, *GCB Bioenergy*, 8, 211–225, <https://doi.org/10.1111/gcbb.12257>, 2016.
- 995 Mozaffar, A., Schoon, N., Digrado, A., Bachy, A., Delaplace, P., Du Jardin, P., Fauconnier, M.-L., Aubinet, M., Heinesch, B., and Amelynck, C.: Methanol emissions from maize: Ontogenetic dependence to varying light conditions and guttation as an additional factor constraining the flux, *Atmospheric Environment*, 152, 405–417, <https://doi.org/10.1016/j.atmosenv.2016.12.041>, 2017.
- Mozaffar, A., Schoon, N., Bachy, A., Digrado, A., Heinesch, B., Aubinet, M., Fauconnier, M.-L., Delaplace, P., du Jardin, P., and Amelynck, C.: Biogenic volatile organic compound emissions from senescent maize leaves and a comparison with other leaf developmental stages, *Atmospheric Environment*, 176, 71–81, <https://doi.org/10.1016/j.atmosenv.2017.12.020>, 2018.
- 1000 Müller, K., Pelzing, M., Gnauk, T., Kappe, A., Teichmann, U., Spindler, G., Haferkorn, S., Jahn, Y., and Herrmann, H.: Monoterpene emissions and carbonyl compound air concentrations during the blooming period of rape (*Brassica napus*), *Chemosphere*, 49, 1247–1256, [https://doi.org/10.1016/S0045-6535\(02\)00610-0](https://doi.org/10.1016/S0045-6535(02)00610-0), 2002.
- 1005 Niinemets, U., Loreto, F., Reichstein, M.: Physiological and physicochemical controls on foliar volatile organic compound emissions. *Trends Plant Sci.* 9, 180–186, 2004.
- NIST database, 2023, <https://webbook.nist.gov/chemistry/>, last consulted 19/09/2023.
- 1010 Pagonis, D., Sekimoto, K., de Gouw, J.: A Library of Proton-Transfer Reactions of H₃O⁺ Ions Used for Trace Gas Detection, *J. Am. Soc. Mass Spectrom.* 30, 1330–1335, doi: 10.1007/s13361-019-02209-3, 2019.
- Park, J.-H., Goldstein, A. H., Timkovsky, J., Fares, S., Weber, R., Karlik, J., and Holzinger, R.: Eddy covariance emission and deposition flux measurements using proton transfer reaction – time of flight – mass spectrometry (PTR-TOF-MS): comparison with PTR-MS measured vertical gradients and fluxes, *Atmos. Chem. Phys.*, 13, 1439–1456, <https://doi.org/10.5194/acp-13-1439-2013>, 2013.
- 1015 Park, J.-H., Fares, S., Weber, R., and Goldstein, A. H.: Biogenic volatile organic compound emissions during BEARPEX 2009 measured by eddy covariance and flux–gradient similarity methods, *Atmos. Chem. Phys.*, 14, 231–244, <https://doi.org/10.5194/acp-14-231-2014>, 2014.
- Peñuelas, J. and Staudt, M.: BVOC and global change, *Trends in Plant Science*, 15, 133–144, <https://doi.org/10.1016/j.tplants.2009.12.005>, 2010.
- 1020 Piesik, D., Pańka, D., Delaney, K. J., Skoczek, A., Lamparski, R., and Weaver, D. K.: Cereal crop volatile organic compound induction after mechanical injury, beetle herbivory (*Oulema* spp.), or fungal infection (*Fusarium* spp.), *Journal of Plant Physiology*, 168, 878–886, <https://doi.org/10.1016/j.jplph.2010.11.010>, 2011.
- Rottenberger, S., Kuhn, U., Wolf, A., Schebeske, G., Oliva, S.T., Tavares, T.M., Kesselmeier, J.: Formaldehyde and acetaldehyde exchange during leaf development of the Amazonian deciduous tree species *Hymenaea courbaril*, *Atmospheric Environment*, 39, 2275–2279, doi:10.1016/j.atmosenv.2004.12.027, 2005.
- 1025 Ruuskanen, T. M., Müller, M., Schnitzhofer, R., Karl, T., Graus, M., Bamberger, I., Hörtnagl, L., Brilli, F., Wohlfahrt, G., and Hansel, A.: Eddy covariance VOC emission and deposition fluxes above grassland using PTR-TOF, *Atmos. Chem. Phys.*, 11, 611–625, <https://doi.org/10.5194/acp-11-611-2011>, 2011.



- 1030 Sakulyanontvittaya, T., Guenther, A., Helmig, D., Milford, J., and Wiedinmyer, C.: Secondary Organic Aerosol from Sesquiterpene and Monoterpene Emissions in the United States, *Environ. Sci. Technol.*, 42, 8784–8790, <https://doi.org/10.1021/es800817r>, 2008.
- Salazar Gómez, J.I., Klucken, C., Sojka, M., Masliuk, L., Lunkenbein, T., Schlögl, R., Ruland, H.: Elucidation of artefacts in proton transfer reaction time-of-flight mass spectrometers, *J Mass Spectrom.*, 54, 987–1002, 2019.
- 1035 Salazar Gómez, J.I., Sojka, M., Klucken, C., Schlögl, R., Ruland, H.: Determination of trace compounds and artifacts in nitrogen background measurements by proton transfer reaction time-of-flight mass spectrometry under dry and humid conditions, *J Mass Spectrom.*, 56:e4777, <https://doi.org/10.1002/jms.4777>, 2021.
- 1040 Sarkar, C., Guenther, A.B., Park, J.-H., Seco, R., Aalves, E., Batalha, S., Santana, R., Kim, S., Smith, J., Tóta, J., and Vega, O.: PTR-TOF-MS eddy covariance measurements of isoprene and monoterpene fluxes from an eastern Amazonian rainforest, *Atmos. Chem. Phys.*, 20, 7179–7191, <https://doi.org/10.5194/acp-20-7179-2020>, 2020.
- Sartelet, K. N., Couvidat, F., Seigneur, C., and Roustan, Y.: Impact of biogenic emissions on air quality over Europe and North America, *Atmospheric Environment*, 53, 131–141, <https://doi.org/10.1016/j.atmosenv.2011.10.046>, 2012.
- Schallhart, S., Rantala, P., Nemitz, E., Taipale, D., Tillmann, R., Mentel, T.F., Loubet, B., Gerosa, G., Finco, A., Rinne, J., and Ruuskanen, T.M.: Characterization of total ecosystem-scale biogenic VOC exchange at a Mediterranean oak–hornbeam forest, *Atmos. Chem. Phys.*, 16, 7171–7194, doi:10.5194/acp-16-7171-2016, 2016.
- 1050 Schallhart, S., Rantala, P., Kajos, M.K., Aalto, J., Mammarella, I., Ruuskanen, T.M., and Kulmala, M.: Temporal variation of VOC fluxes measured with PTR-TOF above a boreal forest, *Atmos. Chem. Phys.*, 18, 815–832, <https://doi.org/10.5194/acp-18-815-2018>, 2018.
- 1055 Seco, R., Peñuelas, J., and Filella, I.: Short-chain oxygenated VOCs: Emission and uptake by plants and atmospheric sources, sinks, and concentrations, *Atmospheric Environment*, 41, 2477–2499, <https://doi.org/10.1016/j.atmosenv.2006.11.029>, 2007.
- Seco, R., Holst, T., Matzen, M.S., Westergaard-Nielsen, A., Li, T., Simin, T., Jansen, J., Crill, P., Friborg, T., Rinne, J., and Rinnan, R.: Volatile organic compound fluxes in a subarctic peatland and lake, *Atmos. Chem. Phys.*, 20, 13399–13416, <https://doi.org/10.5194/acp-20-13399-2020>, 2020.
- 1060 Sindelarova, K., Granier, C., Bouarar, I., Guenther, A., Tilmes, S., Stavrakou, T., Müller, J.-F., Kuhn, U., Stefani, P., and Knorr, W.: Global data set of biogenic VOC emissions calculated by the MEGAN model over the last 30 years, *Atmos. Chem. Phys.*, 14, 9317–9341, <https://doi.org/10.5194/acp-14-9317-2014>, 2014.
- Spirig, C., Neftel, A., Ammann, C., Dommen, J., Grabmer, W., Thielmann, A., Schaub, A., Beauchamp, J., Wisthaler, A., and Hansel, A.: Eddy covariance flux measurements of biogenic VOCs during ECHO 2003 using proton transfer reaction mass spectrometry, *Atmos. Chem. Phys.*, 5, 465–481, <https://doi.org/10.5194/acp-5-465-2005>, 2005.
- Stevenson, D. S., Zhao, A., Naik, V., O’Connor, F. M., Tilmes, S., Zeng, G., Murray, L. T., Collins, W. J., Griffiths, P. T., Shim, S., Horowitz, L. W., Sentman, L. T., and Emmons, L.: Trends in global tropospheric hydroxyl radical and methane lifetime since 1850 from AerChemMIP, *Atmos. Chem. Phys.*, 20, 12905–12920, <https://doi.org/10.5194/acp-20-12905-2020>, 2020.
- 1070 Verhoef, A., McNaughton, K. G., and Jacobs, A. F. G.: A parameterization of momentum roughness length and displacement height for a wide range of canopy densities, *Hydrol. Earth Syst. Sci.*, 1, 81–91, 10.5194/hess-1-81-1997, 1997.
- Veromann, E., Toome, M., Kännaste, A., Kaasik, R., Copolovici, L., Flink, J., Kovács, G., Narits, L., Luik, A., and Niinemets, Ü.: Effects of nitrogen fertilization on insect pests, their parasitoids, plant diseases and volatile organic compounds in *Brassica napus*, *Crop Protection*, 43, 79–88, <https://doi.org/10.1016/j.cropro.2012.09.001>, 2013.
- Vivaldo, G., Masi, E., Taiti, C., Caldarelli, G., and Mancuso, S.: The network of plants volatile organic compounds, *Sci Rep*, 7, 11050, <https://doi.org/10.1038/s41598-017-10975-x>, 2017.
- 1080 Voyard, A., Ciuraru, R., Lafouge, F., Décuq, C., Fortineau, A., Loubet, B., Staudt, M., Rees, F.: Emissions of volatile organic compounds from aboveground and belowground parts of rapeseed (*Brassica napus* L.) and tomato (*Solanum lycopersicum* L.), *Sci. Total Environ.*, 955, 177081, <https://doi.org/10.1016/j.scitotenv.2024.177081>, 2024.
- 1085 Vuolo, R. M., Loubet, B., Mascher, N., Gueudet, J.-C., Durand, B., Laville, P., Zurfluh, O., Ciuraru, R., Stella, P., and Trebs, I.: Nitrogen oxides and ozone fluxes from an oilseed-rape management cycle: the influence of cattle slurry application, *Biogeosciences*, 14, 2225–2244, <https://doi.org/10.5194/bg-14-2225-2017>, 2017.
- Wiß, F., Ghirardo, A., Schnitzler, J.-P., Nendel, C., Augustin, J., Hoffmann, M., and Grote, R.: Net ecosystem fluxes and composition of biogenic volatile organic compounds over a maize field–interaction of meteorology and phenological stages, *GCB Bioenergy*, 9, 1627–1643, <https://doi.org/10.1111/gcbb.12454>, 2017.
- 1090



- Woźniak, E., Waszkowska, E., Zimny, T., Sowa, S., and Twardowski, T.: The Rapeseed Potential in Poland and Germany in the Context of Production, Legislation, and Intellectual Property Rights, *Front. Plant Sci.*, 10, 1423, <https://doi.org/10.3389/fpls.2019.01423>, 2019.
- 1095 Xue, J., Ma, F., Elm, J., Chen, J., and Xie, H.-B.: Atmospheric Oxidation Mechanism and Kinetics of Indole Initiated by $\cdot\text{OH}$ and $\cdot\text{Cl}$: A Computational Study, *Atmos. Chem. Phys.*, 22, 11543–11555, <https://doi.org/10.5194/acp-22-11543-2022>, 2022.
- 1100 Yáñez-Serrano, A. M., Filella, I., LLusà, J., Gargallo-Garriga, A., Granda, V., Bourtsoukidis, E., Williams, J., Seco, R., Cappellin, L., Werner, C., de Gouw, J., and Peñuelas, J.: GLOVOCS - Master compound assignment guide for proton transfer reaction mass spectrometry users, *Atmospheric Environment*, 244, 117929, <https://doi.org/10.1016/j.atmosenv.2020.117929>, 2021.